


# Preliminary Study on Pharmacokinetics and Antitumor Pharmacodynamics of Folic Acid Modified Crebanine Polyethyleneglycol-Polylactic Acid Hydroxyacetic Acid Copolymer Nanoparticles

Xin Cheng <sup>1-4,\*</sup>, Rui Pan<sup>1,3-5,\*</sup>, Junze Tang<sup>1,4</sup>, Kun Yu<sup>1,4</sup>, Hailiang Zhang<sup>1,3-5</sup>, Xiaoyu Zhao<sup>1,4</sup>

<sup>1</sup>College of Traditional Chinese Medicine, Yunnan University of Chinese Medicine, Kunming, 650500, People's Republic of China; <sup>2</sup>The Key Laboratory of External Drug Delivery System and Preparation Technology in University of Yunnan Province, Kunming, 650500, People's Republic of China; <sup>3</sup>Yunnan Key Laboratory of Dai and Yi Medicines, Kunming, 650500, People's Republic of China; <sup>4</sup>Laboratory Animal Center, Yunnan University of Chinese Medicine, Kunming, 650500, People's Republic of China; <sup>5</sup>College of Chinese Materia Medica and Yunnan Key Laboratory of Southern Medicinal Utilization, Kunming, 650500, People's Republic of China

\*These authors contributed equally to this work

Correspondence: Xin Cheng, Yunnan University of Chinese Medicine, Chenggong District, Kunming City, Yunnan Province, People's Republic of China, Tel +861 598 716 2031, Email chengxin920@126.com

**Purpose:** Liver cancer is associated significantly with morbidity and mortality. The combination of low-intensity ultrasound with nanomedicine delivery systems holds promise as an alternative for the treatment for liver cancer. This study focuses on the utilization of folic acid (FA) modified nanoparticles, which are loaded with fluorescent dye DiR and liquid fluorocarbon (PFP). These nanoparticles have the potential to enhance liver cancer targeting under ultrasound stimulation and future applications in vivo.

**Methods:** The pharmacokinetics and tissue distribution of folic acid-modified Crebanine polyethylene glycol-poly(lactic acid) copolymer nanoparticles (FA-Cre@PEG-PLGA NPs) were investigated. The pharmacokinetic parameters, liver targeting, and in vivo distribution were assessed. Additionally, the inhibitory impacts of FA-Cre@PEG-PLGA NPs in combination with ultrasonic irradiation on the proliferation and acute toxicity of H22 cells of mouse hepatoma were investigated in vitro. The tumor targeting and anti-tumor efficacy of FA-Cre@PEG-PLGA NPs were assessed utilizing a small animal in vivo imaging system and an in situ hepatocellular carcinoma transplantation model, respectively.

**Results:** The pharmacokinetic studies and tissue distribution tests demonstrated that FA-Cre@PEG-PLGA NPs conspicuously prolonged the half-life and retention time of the drug in rats, and the liver targeting effect was pronounced. Additionally, the in vivo acute toxicity test indicated that FA-Cre@PEG-PLGA NPs had minimal adverse reactions and could fulfill the aim of attenuating the drug. The outcomes of the animal experiments further substantiated that FA-Cre@PEG-PLGA NPs had a longer retention time at the tumor site, a superior anti-tumor effect, and less damage to liver and kidney tissue.

**Conclusion:** The integration of FA-Cre@PEG-PLGA NPs with ultrasound irradiation demonstrated exceptional safety and potent anti-tumor efficacy in vivo, presenting a promising therapeutic strategy for the treatment of liver cancer through the combination of ultrasound technology with a nanomedicine delivery system.

**Keywords:** targeted drug delivery, pharmacokinetics, ultrasound irradiation, antitumor activity

## Introduction

Cancer has always posed a formidable challenge to humanity, having a profound impact on human health and imposing an enormous financial burden on patients and their families. The result is that it has emerged as an undeniable social problem that demands immediate attention. Primary liver cancer, a malignant neoplasm originating in the digestive

system of the liver, ranks sixth globally in annual incidence and third in mortality, according to the American Cancer Society.<sup>1,2</sup>

Hepatocellular carcinoma (HCC) accounts for approximately 75% of all primary liver cancers, while cholangiocarcinoma arising from bile duct epithelium is relatively rare occurrences.<sup>3,4</sup> While surgical resection remains the cornerstone treatment for liver cancer, its high-risk profile, the substantial physical trauma inflicted on the patient, and elevated postoperative recurrence rates significantly limit its clinical applicability.<sup>5–7</sup> In addition, conventional therapeutic modalities such as chemotherapy, liver transplant, and ablation have shown limited efficacy with respect to HCC treatment outcomes and prognosis improvement.<sup>8</sup> Hence, the urgent need for novel drugs that, alongside innovative therapeutic approaches, boast minimal toxic side effects coupled with potent anti-tumor activity.<sup>9–11</sup>

In recent years, targeted drug delivery systems have emerged as a promising approach for specific accumulation of drugs at tumor sites, offering distinct advantages over conventional drug therapies. Consequently, they have garnered significant attention in the field of early diagnosis and precise treatment of liver cancer.<sup>12–14</sup> Block copolymer micelles are nanoscale aggregates formed through the self-assembly of amphiphilic polymers, with hydrophobic cores encapsulated by hydrophilic shells serving as drug containers to enhance water solubility and drug efficacy.<sup>15–18</sup> Polyethylene glycol (PEG) exhibits excellent hydrophilicity, prolongs the circulation and retention time of drugs within the body, and boosts stability.<sup>19</sup> Polylactic acid-glycolic acid (PLGA) possesses good biocompatibility and safety and can be degraded into non-toxic products *in vivo*, which can effectively enhance the solubility, dissolution, drug efficacy, and other parameters of insoluble drugs.<sup>20–23</sup> Hence, the PEG-PLGA copolymer carrier augments the stability of the carrier, extends the systemic circulation time, ameliorates the release kinetic characteristics of the drug, and heightens the drug efficacy.<sup>24,25</sup> The abundant expression of receptors in cancer cells has rendered folic acid (FA) a widely employed constituent in targeted drug delivery systems.<sup>26,27</sup> Folate enters normal tissue cells primarily through the transmembrane pathway. However, it selectively binds to folate receptors (FR) that are overexpressed across various cancer types and exhibit a remarkable affinity towards FA-mediated internalization into cancer cells.<sup>28,29</sup> In order to achieve a dual targeting system encompassing both passive and active mechanisms, the carboxyl group of the folic acid molecule undergoes chemical modification to establish an intricate connection with the amino terminal of the PEG within the PEG-PLGA construction. Thus, in obtaining a targeted carrier named polyethylene glycol-poly(lactic acid) hydroxyacetic acid-folic acid (PEG-PLGA-FA), which effectively mitigates toxicities and side effects associated with conventional drug therapies while promoting enhanced drug accumulation at tumor sites.

The utilization of ultrasound imaging (US) in diagnostic imaging is widespread due to its physical properties, cost-effectiveness, safety, and non-invasive nature. Additionally, the ultrasonic cavitation effect and thermal radiation effect can induce thermal or mechanical effects that facilitate drug release from nanoparticles.<sup>30–33</sup> Moreover, ultrasound enhances the instantaneous permeability of blood vessels and increases cellular uptake by facilitating drug transfer from liquid fluorocarbon (PFP) nanobubbles to neighboring tumor cells through phase shift induced by a specific intensity of ultrasonic irradiation. This approach not only improves therapeutic efficacy but also inhibits tumor cell metastasis.<sup>34,35</sup> As a result, the combination of low-intensity ultrasound with nanomedicine delivery systems has emerged as a promising alternative to cancer therapy. In our previous study, we prepared FA-Cre@PEG-PLGA NPs by encapsulating Crebanine in PEG-PLGA nanoparticles modified with folic acid. We investigated the *in vitro* anti-tumor effect of combined ultrasonic irradiation on BEL-7402 liver cancer cells and observed significant enhancements in proliferation inhibition rate, anti-tumor migration ability, and cellular uptake.<sup>36</sup>

In this study, a low-intensity ultrasound in combination with a nanomedicine delivery system was introduced. It was affirmed by pharmacokinetic studies that FA-Cre@PEG-PLGA NPs can enhance the circulation time and bioavailability of the drug *in vivo*. Moreover, tissue distribution studies indicated that it possesses liver targeting. *In vivo* small animal imaging (IVIS) in conjunction with ultrasound therapy was employed to establish a quantitative fluorescence image analysis method for evaluating the tumor targeting ability of FA-Cre@PEG-PLGA NPs. It demonstrated significant tumor inhibition *in situ* hepatocellular carcinoma transplantation model. The targeted drug delivery of FA-Cre@PEG-PLGA NPs under the guidance of low-intensity ultrasound not only exhibits low toxicity, low side effects and a favorable anti-tumor effect but also has an imaging function, facilitating the monitoring and diagnosis of tumor progression and providing a promising strategy for the subsequent diagnosis and adjuvant therapy of liver cancer (Figure 1).

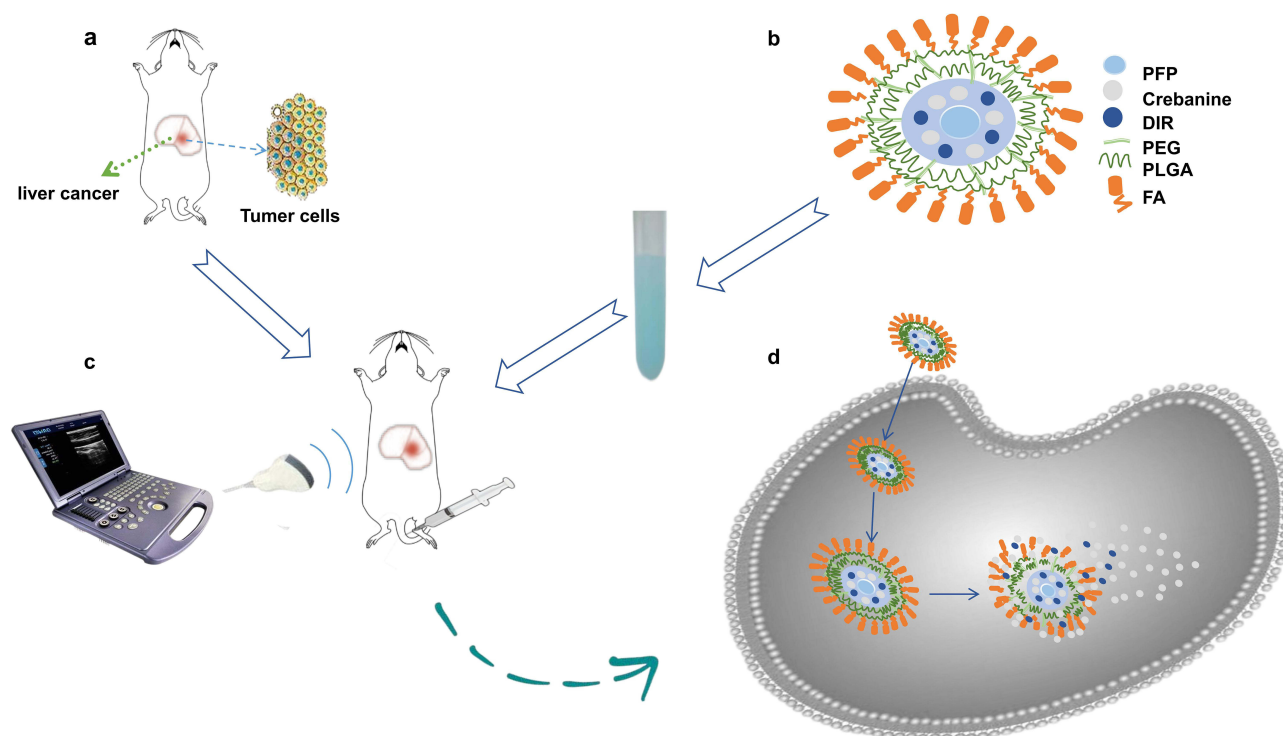


**Figure 1** Combined application of FA-Cre@PEG-PLGA NPs and ultrasound imaging for precise treatment of hepatocellular carcinoma in mice (schematic).

**Notes:** (a) Establishment of an orthotopic transplantation tumor model of hepatocellular carcinoma in mice. (b) Intravenous administration of meticulously prepared FA-Cre@PEG-PLGA NPs. (c) Ultrasonic irradiation treatment. (d) FA-Cre@PEG-PLGA NPs enters the tumor tissue, and ultrasonic blasting releases Crebanine and DiR.

## Materials and Methods

### Materials

The FA-Cre@PEG-PLGA NPs (prepared by the Pharmaceutical Laboratory of Yunnan University of Chinese Medicine) with Crebanine content of 6mg/mL and an encapsulation rate of 83.78% were obtained. The particle size is  $(247.67 \pm 2.49)$  nm, and the Zeta potential is  $(-9.40 \pm 0.54)$  mV. Heparin sodium injection was purchased from Changzhou Qianhong Biochemical Pharmaceutical Co. Ltd. Penicillin-streptomycin (double antibody), fetal bovine serum, PBS phosphate buffer, and RPMI 1640 medium were purchased from Shanghai Date Hill Biotechnology Co. Ltd. The CCK-8 reagent was acquired from Xi'an Ruixi Biological Technology Co. Ltd, while additional organic solvents used were of high-performance liquid chromatography (HPLC) grade, sourced from Thermo Company in the United States.

### Animals

The male Sprague-Dawley rats weighing 230–250 g and the male Kunming mice weighing 18–22 g were procured from SPF (Beijing, China) Biotechnology Co. Ltd. All the animals were housed at the Experimental Animal Center with Yunnan University of Chinese Medicine. The protocols for using animals in this study were approved by the Animal Experimental Ethics Review Committee of Yunnan University of Chinese Medicine (Kunming, China) (R-062022082, R-062023114). All experimental proceedings were conducted in compliance with the “Laboratory Animal Guideline for Ethical Review of Animal Welfare (GB/T 35892–2018)”.

## In vivo Pharmacokinetics Study

### Experimental Design

Male Sprague-Dawley rats weighing 230–250 g were randomly assigned into two groups ( $n = 6$ ) following a 12 hours fasting period: the FA-Cre@PEG-PLGA NPs group and the Crebanine bulk drug group received a single dose of the respective drug at a concentration of 3 mg/kg via tail vein injection. Subsequently, blood samples were collected through

orbital blood collection at predetermined time intervals (5, 15, 30, 60, 180, 360, 600, 720, and 960 minutes). The collected blood samples were subsequently placed in a centrifuge tube with heparin sodium, which were centrifuged at a speed of approximately 6000 r/min for 10 minutes at 4°C to obtain approximately 300 µL aliquots. These aliquots were subsequently stored at –80°C until further analysis using HPLC.

### Pre-Treatment of the Plasma Samples

In plasma sample preparation, a 20 µL solution of verapamil (internal standard) was added to the 200 µL plasma sample and vortexed for 3 minutes. Subsequently, 1.2 mL acetonitrile was added and allowed to stand for 5 minutes before being centrifuged at 6000 r/min for 10 minutes at 4°C. The resulting supernatant (1.0 mL) was collected. The supernatant was then dried using a nitrogen blower (HSC-12A, Tianjin Hengao Technology Development Company), followed by addition of 200 µL methanol and vortexed for 3 minutes to redissolve it. Finally, the mixture was filtered through a microporous filter membrane with a pore size of 0.22 µm. The filtrate 100 µL was sampled for HPLC analysis, and it was ascertained that the peak regions A1 corresponding to the Crebanine and A2 corresponding to the internal standard verapamil solution. The ratio of these peak areas ( $A = A1/A2$ ) was substituted into the regression equation derived from the standard curve in order to calculate the blood concentration of Crebanine in rats at each time point studied. Pharmacokinetic parameters were calculated using DAS 3.0 software.

### Analysis Method

HPLC analysis was performed using an Agilent system equipped with Diamonsil C18 column (5 µm, 250 × 4.6 nm) while maintaining the column temperature at 30°C. The mobile phase consisted of methanol (A) and 0.2% triethylamine solution (B), with an A: B ratio of 75:25. Detection was performed at a wavelength of 280 nm, with a flow rate of 1 mL/min and the injected volume of 10 µL.

### Method Validation

The reliability of the HPLC method is verified by evaluating its specificity, linearity, quantization limit, accuracy, stability and recovery rate.

### Tissue Distribution

For the investigation of tissue distribution, male SD rats weighing 230–250 g were randomly divided into two groups (n = 24): The FA-Cre@PEG-PLGA NPs group and the Crebanine bulk drug group received a single intravenous injection of 3 mg/kg of the respective drug through the tail vein. Samples of heart, liver, spleen, lung, kidney, and brain tissues were collected at specified time points after euthanasia (30, 60, 120, 240 minutes), followed by rinsing with normal saline and drying using filter paper. Tissue samples were processed according to the method described under “Pre-treatment of Plasma Samples” and then injected for analysis following the “Analysis Method”. The Crebanine content was quantified in each tissue sample. Maximum peak concentration ratio ( $C_e$ ), selectivity index ( $S_i$ ), relative uptake rate peak concentration ratio ( $Re$ ), and targeting efficiency ( $Te$ ) were employed to evaluate the targeting ability of FA-Cre@PEG-PLGA NPs (Equations 1–4).

$$C_e = \frac{(C_{max})_N}{(C_{max})_D} \quad (1)$$

where  $(C_{max})_N$  and  $(C_{max})_D$  represent the peak mass concentrations of FA-Cre@PEG-PLGA NPs and Crebanine bulk drug, respectively.

$$S_i = \frac{C_N}{C_D} \quad (2)$$

where  $C_N$  and  $C_D$  denote the mass concentrations of FA-Cre@PEG-PLGA NPs and Crebanine bulk drugs at different time intervals.

$$Re = \frac{AUC_N}{AUC_D} \quad (3)$$



where the footpoints N and D refer to FA-Cre@PEG-PLGA NPs and Crebanine bulk drugs, respectively, the AUC value represents the area under the drug concentration–time curve computed from the drug time curve.

$$T_e = \frac{AUC_{Liver}}{AUC_{Other\ tissues}} \quad (4)$$

### Acute Toxicity in vivo

Male KunMing mice weighing 18–22 g were randomly allocated into six groups ( $n = 7$ ) following a 12 hours fasting period: the control group, 2 mg/kg group, 5 mg/kg group, 10 mg/kg group, 15 mg/kg group, and 25 mg/kg group. FA-Cre@PEG-PLGA NPs were prepared at the required concentration for each dose group and administered intravenously. Autonomic activity of mice in each group was closely monitored for more than 6 hours after administration to assess any toxic manifestations and characteristics exhibited by the mice and to determine the onset and recovery time of any toxic response, if present, as well as the mortality rate. In the case of mouse mortality, gross anatomical observations were performed, while the surviving mice were allowed ad libitum access to food and water for 14 days. The daily measurement of mice's body weight after administration allowed for the calculation of the change rate (Equation 5). The resulting post-administration body weight difference was then analyzed and compared to the original measurements. Following this observation period, all surviving mice were euthanized for organ analysis. Heart, liver, spleen, lung and brain tissue from each mouse were dissected and weighed to calculate organ indices (Equation 6). Subsequent fixation with paraformaldehyde followed by embedding in paraffin wax enabled the preparation of HE stained sections, facilitating microscopic examination of pathological changes.

$$\text{Body mass change} = \frac{(\text{Preshent body mass} - \text{Primary body mass})}{\text{Primary body mass}} \quad (5)$$

$$\text{Organ index} = \frac{\text{Organ mass}}{\text{Body mass}} \quad (6)$$

### In vitro and in vivo Ultrasonic Irradiation Methods for FA-Cre@PEG-PLGA NPs

Referring to the work of Tian Y,<sup>37</sup> we aimed to achieve similar outcomes using diagnostic ultrasound and low-intensity focused ultrasound. The ultrasonic diagnostic instrument (DP-50, Shenzhen Mindray Biomedical Electronics Co. Ltd, China) equipped with a convex array probe (35C50EA) was selected for ultrasonic imaging. The normal ultrasound mode is tuned to B mode. Other ultrasonic settings included a frequency of 8.5 MHz, depth of 3.7, and mechanical index (MI) of 0.3. During the in vitro study, the ultrasonic probe was positioned vertically at the bottom of each well plate (96-well), while air interference was eliminated using a coupling adhesive from Tianjin Jinya Technology Development Co. Ltd (20190393). Intermittent ultrasound sessions were performed for each trap for a total irradiation time of 25 minutes. In in vivo studies, ultrasound probes are placed vertically in the liver of tumor-bearing mice. All other conditions remain the same as those used in vitro.

### Cells

Murine hepatocarcinoma cell line H22 was purchased from the China Center for Type Culture Collection (CCTCC, Wuhan, China). The H22 cell line was authenticated by amplification of gene COX1 and electrophoresis, which was provided by Cellcook Biotech Co. Ltd (Guangzhou, China). The cell was cultured in RPMI 1640 medium (VivaCell, #2222741, Date Hill Biotechnology Co. Ltd, Shanghai, China) containing 10% fetal bovine serum (VivaCell, #2144324, Date Hill Biotechnology Co. Ltd, Shanghai, China) and 1% penicillin-streptomycin (PS) (VivaCell, #20010335, Date Hill Biotechnology Co. Ltd, Shanghai, China) and maintained at a 37°C in a 5% CO<sub>2</sub> incubator.

### Cell damage test by ultrasonic irradiation

Ultrasonic and non-ultrasonic groups were established. Methods: H22 cells in the logarithmic growth phase were seeded onto 96-well plates at a density of  $1 \times 10^4$  cells per hole. The ultrasonic group was subjected to ultrasonic irradiation for

24 hours, followed by the addition of 10  $\mu$ L CCK-8 solution and additional incubation for 24 and 48 hours, respectively. After an additional culture period of 2 hours, the absorbance (A) value was measured at a wavelength of 450 nm using an enzyme labeler. The treatment procedure in the non-ultrasound group was identical to that in the ultrasound group, except for the absence of ultrasound exposure. The cell mortality rate after ultrasonic irradiation was calculated as follows (Equation 7).

$$\text{Cell mortality} = \frac{(A_{\text{non-ultrasonic group}} - A_{\text{ultrasonic group}})}{A_{\text{ultrasonic group}}} \quad (7)$$

## In vitro Cytotoxicity

CCK-8 was used to evaluate the rate of proliferation inhibition in H22 cells with both the Crebanine bulk drug and FA-Cre@PEG-PLGA NPs. Ultrasound group: hepatocellular carcinoma H22 cells were inoculated into 96-well plates (density  $1 \times 10^4$ ) during the growth period, given different mass concentrations of Crebanine bulk drugs and FA-Cre@PEG-PLGA NPs, set up control holes (without Crebanine) and blank holes (without Crebanine and cells), plus ultrasound irradiation. In the non-ultrasonic group, except for the absence of ultrasound irradiation, the other conditions remain unchanged. After incubation for 24 and 48 hours, CCK-8 was added to 10  $\mu$ L and continued to be cultured for 2 hours. A value was read at 450 nm wavelength. Untreated cells with 100% cell viability were used as controls. GraphPad Prism 8 software was used to calculate the half-maximal inhibitory concentration ( $IC_{50}$ ). The rate of cell proliferation suppression is calculated using the following equation (Equation 8).

$$\text{Cell proliferation inhibition rate} = \frac{(A_{\text{control}} - A_{\text{test}})}{(A_{\text{control}} - A_{\text{blank}})} \quad (8)$$

## Animal Models

H22 cells were expanded in mice through intraperitoneal injection of H22 cells (density  $5 \times 10^7$ ), and subsequently, H22 ascites cells (density  $1 \times 10^7$ ) were inoculated into the left lobe of the liver to establish a mouse model for orthotopic hepatoma transplantation.

## In vivo Targeting

We previously prepared FA-Cre@PEG-PLGA NPs coated with DiR to evaluate the distribution and tumor targeting efficacy of FA-Cre@PEG-PLGA NPs in mice with orthotopic hepatoma. The mice were randomly divided into two groups: FA-Cre@PEG-PLGA NPs group and FA-Cre@PEG-PLGA NPs combined with ultrasound irradiation group. A dose of 3 mg/kg of FA-Cre@PEG-PLGA NPs was administered via the tail vein. The mice were anesthetized with isoflurane at 0.5, 1, 2, 4, 8, 24, 48, and 72 hours before and after administration, and the distribution and intensity of the fluorescence signal were observed using IVIS spectroscopy. After 72 hours, all mice were humanely euthanized to extract tumor tissue and organs including abdominal wall tumors, heart, liver, spleen, lung and brain for in vitro fluorescence imaging analysis. Simultaneously, the fluorescence intensity was quantified by the IVIS spectroscopy.

To enhance the evaluation of the efficacy of tumor targeting, a matched IVIS imaging system was used to quantify the fluorescence intensity in the whole body and tumor regions during in vivo imaging, and in the tumor and organ regions during in vitro imaging.<sup>38,39</sup> The tumor targeting index (TTI) was calculated using Equation 9 at different time points throughout the in vivo imaging process while for in vitro imaging. Furthermore, the area under the TTI-time curve (AUTC) was calculated based on the trapezoidal rule. Equation 10 was employed to calculate the fluorescence intensity ratio between the tumor and other organs.

$$\text{TTI}\% = \frac{\text{Fluorescence intensity of tumor region}}{\text{Fluorescence intensity of whole body}} \times 100\% \quad (9)$$

$$\text{Intensity ratio} = \frac{\text{Fluorescence intensity of tumor}}{\text{Fluorescence intensity of organ}} \quad (10)$$

## Anti-Tumor in vivo

To evaluate the in vivo anti-tumor effect, three days after modeling completion, the mice were randomly divided into six groups ( $n = 7$ ): No intervention was performed in any treatment group (Blank group), normal saline group (Placebo group), hydroxycamptocampine injection group (HCPT group), Crebanine bulk drug group (Cre group), FA-Cre@PEG-PLGA NPs group (NPs group), and FA-Cre@PEG-PLGA NPs combined with ultrasound irradiation group (NPs+ ultrasound group). The mice received different formulations every other day through the tail vein at doses of 8 mg/kg for HCPT, 3 mg/kg for Cre and NPs. The mice received different preparations at doses of 8 mg/kg HCPT, 3 mg/kg Cre and NPs through the tail vein every other day, and ultrasound was followed by 10 doses in the NPs+ ultrasound group. B-ultrasound imaging using Vetus7 color Doppler ultrasound (Shenzhen Mindray Biomedical Electronics Co. Ltd, China) was performed 24 hours after the last dose. Blood samples were collected for serum biochemical analysis of ALT, AST, BUN, CREA, P21, P27, TNF- $\alpha$ , and IL-6 using an automatic biochemical analyzer (Shenzhen Leidu Life Technology Co. Ltd, China) and ELISA kit (Hanke Biotechnology Co. Ltd, China). Abdominal adhesions, presence of ascites, and abdominal wall tumors were observed. Photographs of the liver were taken, and tumors were weighed to calculate tumor inhibition rate (TGI) (Equation 11). After statistical analysis, it was found that TGI ( $<40\%$ ) did not show effectiveness, while TGI  $\geq 40\%$  and  $P < 0.05$  demonstrated significant effectiveness. The thymus and spleen weights were recorded to calculate the organ index according to (Equation 6). Finally, liver and renal were fixed in 4% paraformaldehyde solutions. The samples were then embedded in paraffin and sectioned and stained with hematoxylin and eosin (H&E) in accordance with standard protocols.

$$\text{TGI} = \frac{(W_{\text{control}} - W_{\text{drug}})}{W_{\text{control}}} * 100\% \quad (11)$$

where  $W_{\text{control}}$  and  $W_{\text{drug}}$  are the tumor weights in drug treated group and control group, respectively.

## Results

### Validation of HPLC Methods for Detection of FA-Cre@PEG-PLGA NPs

The specific results demonstrated (Figure 2a) that under these chromatographic conditions, both Crebanine and internal standard substance exhibited symmetrical peak shapes with excellent separation efficiency, without any interference from endogenous substances, thereby confirming the specificity of the method. The linear relationship results (Figure 2b) indicated a strong correlation between the plasma solution of Crebanine within the concentration range of 0.75 to 48  $\mu\text{g}/\text{mL}$  ( $R^2 = 0.9998$ ), with a lower limit of quantitation mass concentration at 45  $\text{ng}/\text{mL}$ . Intraday precision, daytime precision, and stability all exhibit RSDs below 10%, in addition, the recovery test revealed recoveries greater than 85% for plasma samples across all concentrations, with RSDs less than 6%.

### Integrated Pharmacokinetic Results

The blood concentration time profiles of the Crebanine bulk drug and the FA-Cre@PEG-PLGA NPs following caudal vein injection are plotted in Figure 3. The plasma concentration of Crebanine in the bulk drug group was below detectable levels after 600 minutes of administration, while FA-Cre@PEG-PLGA NPs were detectable for up to 960 minutes. Table 1 summarizes the relevant pharmacokinetic parameters for Crebanine bulk drug and FA-Cre@PEG-PLGA NPs. Both Crebanine bulk drug and FA-Cre@PEG-PLGA NPs conform to the two-compartment model with high correlation coefficients of  $R^2 = 0.9999$  and  $R^2 = 0.9987$ , respectively. The results demonstrate, compared to the Crebanine bulk drug, FA-Cre@PEG-PLGA NPs that exhibited significantly increased AUC,  $t_{1/2\beta}$ , and MRT values ( $P < 0.05$ ), along with a substantial reduction in CL value. Specifically, the AUC of FA-Cre@PEG-PLGA NPs was found to be approximately 2.57 times higher than that of the Crebanine bulk drug. Similarly, the  $T_{1/2\beta}$  value is approximately 1.93 times larger than the Crebanine bulk drug. The MRT and the CL were 1.66 times higher and 0.38 times higher than that

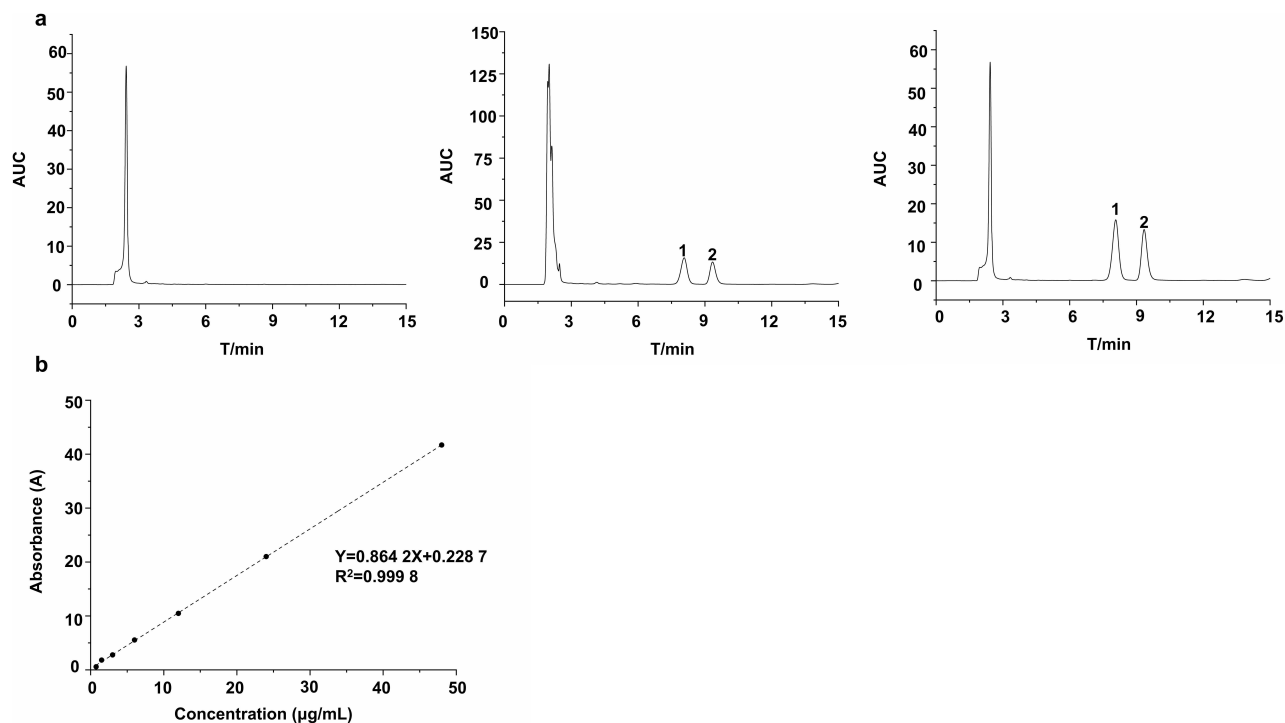


**Figure 2** Method Validation.

**Notes:** (a) From left to right, blank plasma, blank plasma + Crebanine + Internal standard, administered plasma + Internal standard. 1, Crebanine, 2. Internal standard (b) Standard curve of Crebanine in plasma.

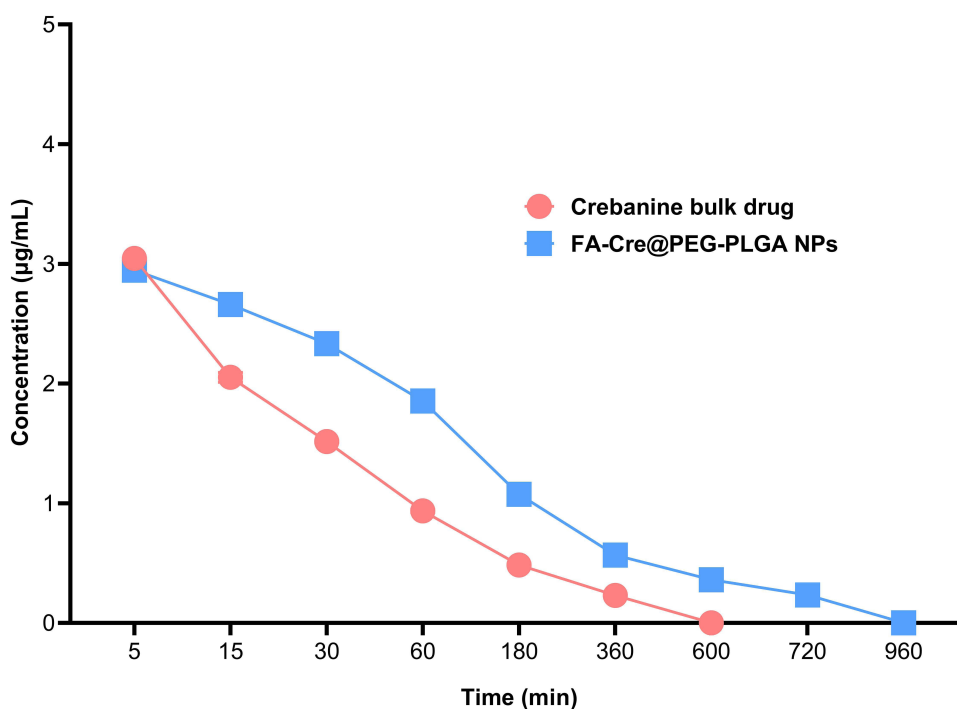


**Figure 3** The mean plasma concentration-time curve of the Crebanine Bulk Drug and the FA-Cre@PEG-PLGA NPs after intravenous injection to rats (mean  $\pm$  SD, n = 5).

of the Crebanine bulk drug. These changes in pharmacokinetic parameters suggest that FA-Cre@PEG-PLGA NPs effectively extend the half-life and retention time of Crebanine in rats while increasing its bioavailability through a sustained-release mechanism.

**Table 1** Pharmacokinetic Parameters of Crebanine in Crebanine Bulk Drug Group, FA-Cre@PEG-PLGA NPs Group (Mean  $\pm$  SD, n = 5)

Argument	Unit	Crebanine Bulk Drug	FA-Cre@PEG-PLGA NPs
AUC <sub>0-t</sub>	$\mu\text{g L}^{-1} \text{h}^{-1}$	4.068 $\pm$ 0.031	10.455 $\pm$ 0.080*
AUC <sub>0-∞</sub>	$\mu\text{g L}^{-1} \text{h}^{-1}$	4.333 $\pm$ 0.025	11.440 $\pm$ 0.100*
MRT <sub>0-t</sub>	h	2.424 $\pm$ 0.016	4.015 $\pm$ 0.010*
MRT <sub>0-∞</sub>	h	3.106 $\pm$ 0.034	5.652 $\pm$ 0.077*
CLz	$\text{L h}^{-1} \text{kg}^{-1}$	692.349 $\pm$ 4.052	262.246 $\pm$ 2.299
$t_{1/2\alpha}$	h	0.916 $\pm$ 0.306	0.724 $\pm$ 0.100
$t_{1/2\beta}$	h	2.035 $\pm$ 0.178	3.930 $\pm$ 0.024*
$K_{10}$	$\text{l h}^{-1}$	0.355 $\pm$ 0.164	0.260 $\pm$ 0.010
$K_{12}$	$\text{l h}^{-1}$	0.402 $\pm$ 0.831	0.230 $\pm$ 0.051
$K_{21}$	$\text{l h}^{-1}$	0.774 $\pm$ 0.826	0.656 $\pm$ 0.059

## Tissue Distribution and Targeting Evaluation of FA-Cre@PEG-PLGA NPs

Tissue distribution results are shown in Figure 4a–d for the Crebanine bulk drug and FA-Cre@PEG-PLGA NPs after intravenous administration in the caudate at a dose of 3 mg/kg. The distribution characteristics of Crebanine bulk drug in various tissues were observed to be lung > liver > kidney > spleen > heart > brain. On the other hand, the distribution pattern of FA-Cre@PEG-PLGA NPs in different tissues showed liver > lung > spleen > kidney > heart > brain between 30 and 120 minutes, and liver > spleen > lung > kidney > heart > brain between 120 and 240 minutes. These findings confirm that FA-Cre@PEG-PLGA NPs primarily target the liver, lungs, and spleen. It has also been observed that Crebanine bulk drugs are primarily metabolized by the liver and excreted through the kidneys. In addition, at 30 minutes post-administration, the concentration of Crebanine was highest in the lungs, whereas for FA-Cre@PEG-PLGA NPs it

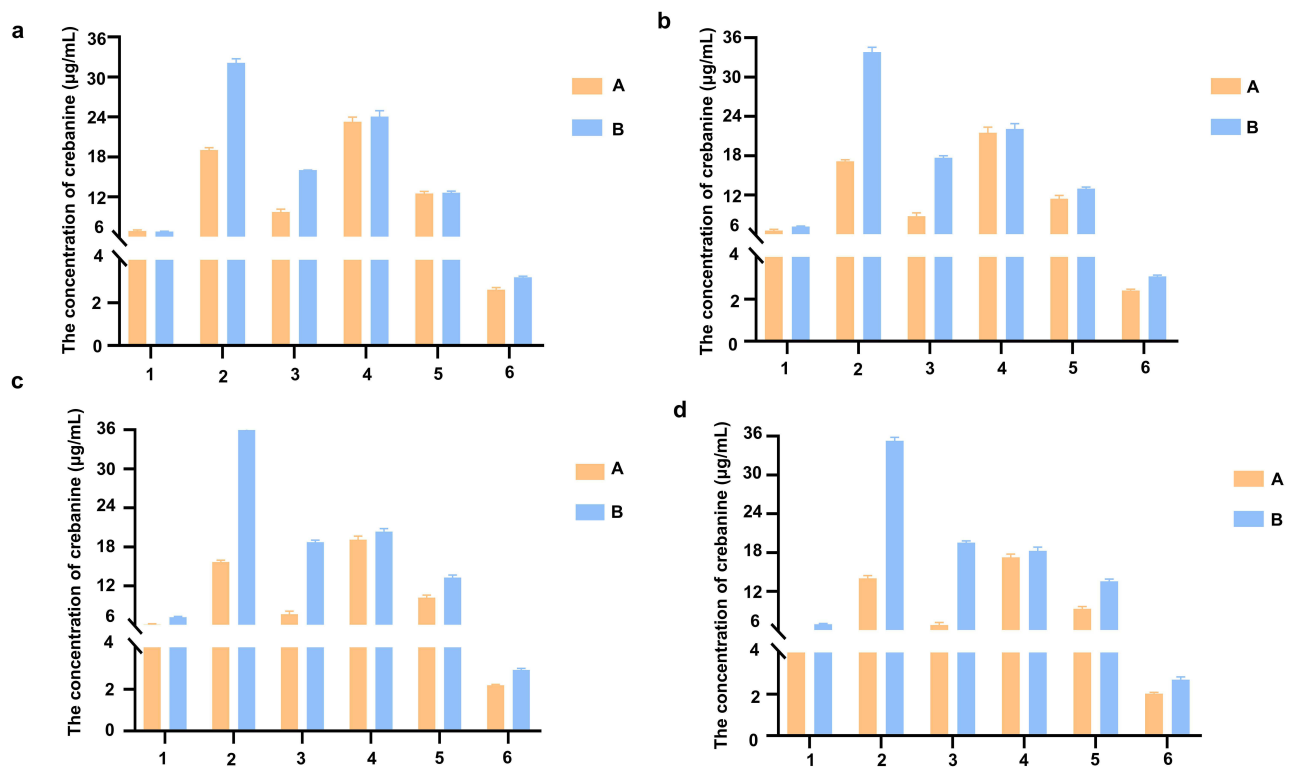


**Figure 4** Distribution of Crebanine bulk drugs and FA-Cre@PEG-PLGA NPs in various tissues at different time points (mean  $\pm$  SD, n = 5).

**Notes:** (a–d) 30, 60, 120 and 240 minutes respectively. A, Crebanine bulk drugs, B, FA-Cre@PEG-PLGA NPs. 1, Heart, 2, Liver, 3, Spleen, 4, Lung, 5, Renal, 6, Brain.



was highest in the liver at this time point. This indicates a gradual accumulation of the drug in the liver over time following nanoparticle preparation, with peak levels reached at 120 minutes. At this time point, the concentration of FA-Cre@PEG-PLGA NPs in the liver was found to be approximately 2.3 times higher than that of Crebanine bulk drug ( $P < 0.01$ ), suggesting enhanced retention and slower decline rate compared to Crebanine bulk drug alone.

To better assess the distribution of FA-Cre@PEG-PLGA NPs in rats, the targeting ability of FA-Cre@PEG-PLGA NPs was evaluated using Ce, Si, Re, and Te. A Ce value greater than 1 and a Re value greater than 1 indicate targeted delivery of the drug formulation to a specific tissue. The results are presented in Table 2 and Table 3. FA-Cre@PEG-PLGA NPs significantly enhanced the peak mass concentration of Crebanine in the liver, demonstrating a significant liver targeting effect. The peak concentration ratio was found to be 1.890 ( $>1$ ), with a relative uptake rate of 2.224 ( $>1$ ). These findings suggest that FA-Cre@PEG-PLGA NPs exhibit strong liver targeting capabilities. Comparing Te values across all tissues revealed that heart, kidney, and brain exhibited Te values  $>2.5$  for FA-Cre@PEG-PLGA NPs, indicating preferential accumulation in the liver compared to Crebanine bulk drug administration alone. In addition, FA-Cre@PEG-PLGA NPs effectively reduced drug accumulation in non-targeted organs. Analysis of Si values at all time points for both FA-Cre@PEG-PLGA NPs and Crebanine bulk drugs demonstrated higher Si values for FA-Cre@PEG-PLGA NPs except in lung tissue. This indicates that the concentration of Crebanine is consistently higher in the liver compared to other tissues/organs throughout all time points examined – highlighting the significant and time-dependent liver targeting effect associated with our nanoparticle formulation specifically.

## Acute Toxicity

Previous studies have demonstrated that Crebanine hydrochloride solution has a relatively elevated toxicity, with a median lethal dose (LD50) of 9.382 mg/kg.<sup>40</sup> Furthermore, an acute toxicity experiment conducted by the previous research group on the Crebanine bulk drugs revealed LD50 of 4.277 mg/kg, which presented a significant obstacle to its development and application due to its extreme toxicity. In order to assess the attenuation effect of FA-Cre@PEG-PLGA

**Table 2** Targeting Tissue Evaluation of FA-Cre@PEG-PLGA NPs

Sample	Re	Ce	Te	
			A	B
Heart	1.153	1.043	2.571	4.960
Liver	2.224	1.890	–	–
Spleen	1.643	2.382	2.025	1.891
Lung	1.051	1.034	0.813	1.719
Renal	1.706	1.278	1.521	2.647
Brain	1.310	1.224	7.090	12.042

Notes: Tables 2, A, Crebanine bulk drugs, B, FA-Cre@PEG-PLGA NPs.

**Table 3** Si Values of Crebanine Bulk Drugs and FA-Cre@PEG-PLGA NPs at Different Time Points

Sample	30 min		60 min		120 min		240 min	
	A	B	A	B	A	B	A	B
Heart	2.772	4.742**	2.615	4.726**	2.579	5.021**	2.459	5.092**
Spleen	1.956	2.007	1.960	1.914	2.053	1.923	2.065	1.805
Lung	0.818	1.335*	0.798	1.532*	0.819	1.768*	0.813	1.933*
Renal	1.521	2.547*	1.501	2.609*	1.539	2.709*	1.509	2.604*
Brain	7.299	10.061**	7.126	10.996**	7.131	12.326**	6.930	13.058**

Notes: Tables 3, A, Crebanine bulk drugs, B, FA-Cre@PEG-PLGA NPs. vs Crebanine bulk drugs, \* $P < 0.05$ , \*\* $P < 0.01$ .

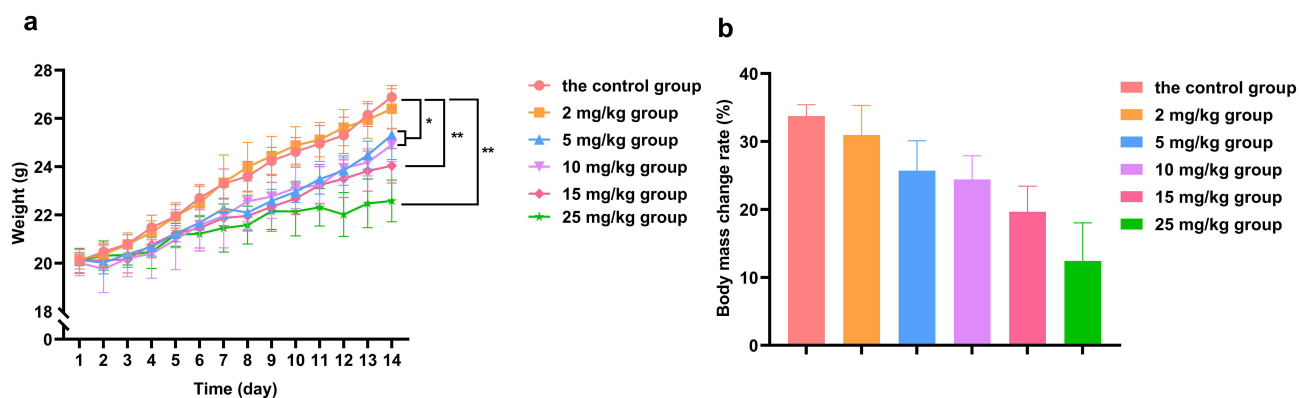


**Figure 5** Body mass change of mice in each group.

**Notes:** (a) body weight, vs the control group, \* $P < 0.05$ , \*\* $P < 0.01$ . (b) body mass change rate.

NPs, an acute toxicity test was performed. In our preliminary experiments, mice injected with 30 mg/kg FA-Cre@PEG-PLGA NPs via the tail vein initially exhibited normal behavior for 30 seconds after injection, however, approximately 35 seconds later, they exhibited tumbling movements, dilated and protruding pupils, tics, urination problems and impaired locomotion. The mice succumbed to the effects within a minute of the injection. The administration of FA-Cre@PEG-PLGA NPs at 25 mg/kg and 15 mg/kg resulted in impaired locomotion resembling intoxication, with convulsions. However, these effects resolve within approximately 60 and 20 minutes, respectively. At a dose of 10 mg/kg of FA-Cre@PEG-PLGA NPs, some mice experienced shortness of breath followed by a quiet rest in the corner of their cage for approximately 30–40 minutes before returning to normal activity levels. Mice given doses of 5 mg/kg and 2 mg/kg FA-Cre@PEG-PLGA NPs showed normal activity with no significant adverse effects. Three mice from the group receiving 25 mg/kg died on the first day of administration, while one mouse from the group receiving 15 mg/kg died on the third day. All the remaining mice survived 14 days under the administration. The body weight of the mice in each group was compared, as shown in Figure 5a and b. On the 14th day post-administration, the body weight of mice in the 2 mg/kg group was  $(26.40 \pm 0.84)$  g ( $P > 0.05$ ), which did not show significant differences when compared to the normal control group. Conversely, the body weight of mice in the 5 mg/kg and 10 mg/kg groups was  $(25.32 \pm 1.03)$  g and  $(24.90 \pm 0.69)$  g, respectively ( $P < 0.05$ ). Furthermore, a notable decrease in body weight was observed for mice treated with doses of 15 mg/kg and 25 mg/kg, resulting in weights of  $(24.04 \pm 0.71)$  g and  $(22.58 \pm 0.86)$  g correspondingly ( $P < 0.01$ ). The body mass change rate in the 2 mg/kg, 5 mg/kg, and 10 mg/kg groups was comparable to that of the normal group, indicating minimal impact on the body weight of mice and low toxicity at these doses. Conversely, the body mass change rate in the 15 mg/kg and 25 mg/kg groups was lower than that of the normal group, supposing greater toxicity at these doses leading to an impact on the body weight of mice. The LD<sub>50</sub> of FA-Cre@PEG-PLGA NPs was calculated by Bilss using SPSS software. Statistical processing showed that the LD<sub>50</sub> of FA-Cre@PEG-PLGA NPs was 22.216 mg/kg, and the toxicity was less than that of Crebanine hydrochloride solution has (9.382 mg/kg) and Crebanine bulk drugs (4.277 mg/kg). The objective of attenuated preparation can be accomplished.

The mice in each group were further dissected, and their organs were removed for weighing, organ index calculation, and HE staining. As shown in Figure 6 and Table 4, mice in groups receiving doses of 10 mg/kg, 15 mg/kg, and 25 mg/kg showed more pronounced effects on the liver and lungs. Inflammatory cell infiltration was observed to varying degrees around hepatic and pulmonary cells. In contrast to the normal group, the tissue cells of the heart, spleen, kidneys and brain in each dose group showed an orderly alignment without any abnormal pathological changes. Myocardial cells and fiber appear normal with well-defined boundaries. No significant lesions or necrosis were observed in the glomerular or tubular structures. The structure of the splenic corpuscles is clearly defined, while the brain cells exhibit organized patterns. These findings suggest that FA-Cre@PEG-PLGA NPs have minimal effects on the heart, spleen, kidneys and brain.

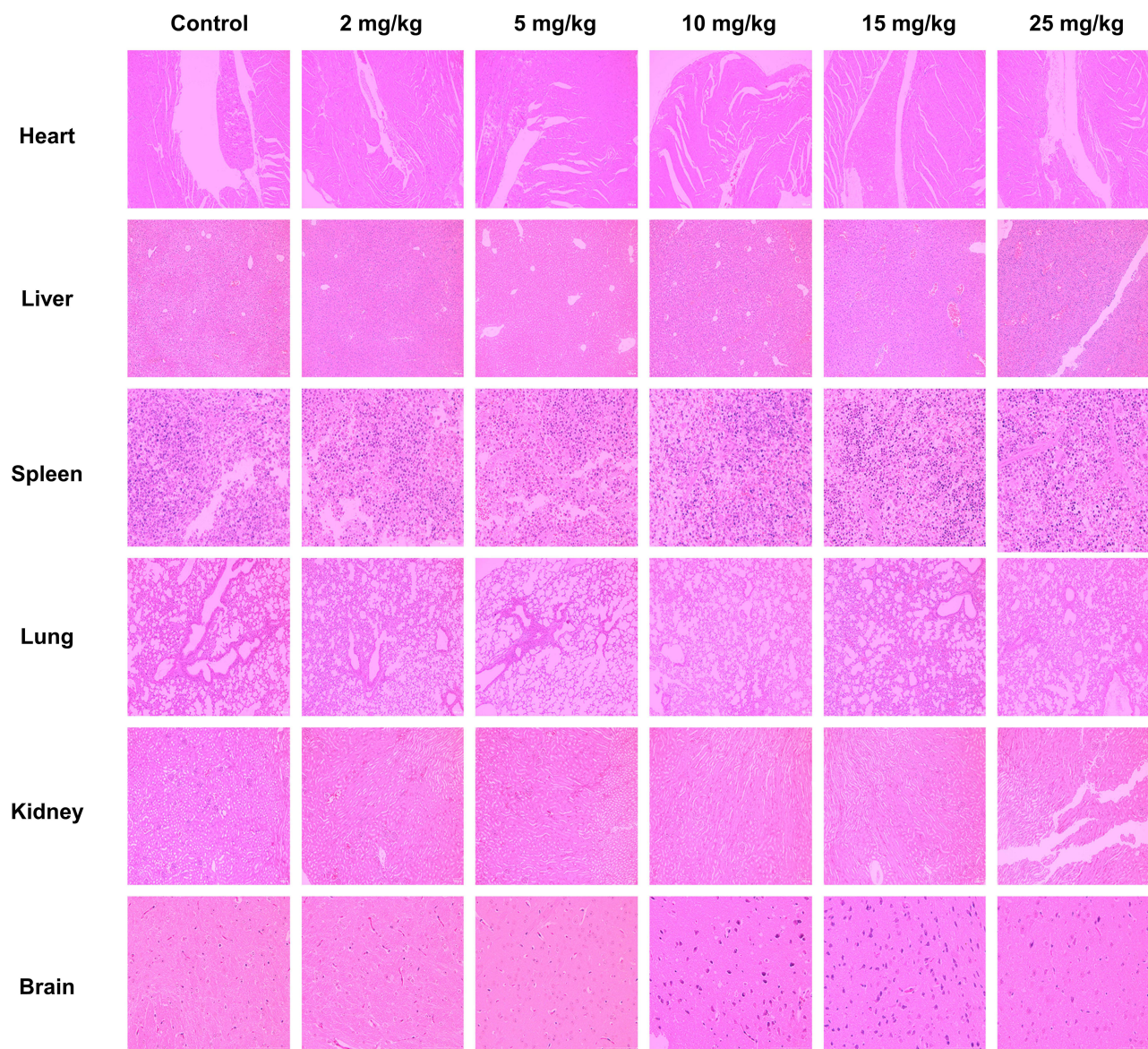


**Figure 6** HE staining was used to detect organs of mice in each group morphology.

## Study on Cell Damage Rate Under in vitro Ultrasound Irradiation

During long-term focused ultrasound for diagnostic antitumor therapy, the temperature of the probe increases, raising safety concerns. To minimize potential harm to normal tissue, precise ultrasonic parameters are crucial. Previous studies have demonstrated that specific ultrasound conditions (frequency: F8.5MHz, depth: d3.7, mechanical index: MI 0.3)

**Table 4** Body Weight and Organ Index of Mice in Each Group (Mean  $\pm$  SD, n = 5)

Group	Heart	Liver	Spleen	Lung	Kidney	Brain
Normal	0.69 $\pm$ 0.05	5.62 $\pm$ 0.26	0.59 $\pm$ 0.02	1.11 $\pm$ 0.10	1.39 $\pm$ 0.09	0.95 $\pm$ 0.06
2 mg/kg	0.69 $\pm$ 0.06	5.49 $\pm$ 0.30	0.58 $\pm$ 0.03	1.08 $\pm$ 0.08	1.35 $\pm$ 0.06	0.96 $\pm$ 0.07
5 mg/kg	0.67 $\pm$ 0.05	5.36 $\pm$ 0.25	0.57 $\pm$ 0.03	1.01 $\pm$ 0.08*	1.35 $\pm$ 0.07	0.95 $\pm$ 0.10
10 mg/kg	0.64 $\pm$ 0.04	5.26 $\pm$ 0.15*	0.57 $\pm$ 0.04	1.01 $\pm$ 0.06*	1.33 $\pm$ 0.09	0.94 $\pm$ 0.08
15 mg/kg	0.63 $\pm$ 0.06	4.76 $\pm$ 0.32**	0.57 $\pm$ 0.05	0.90 $\pm$ 0.04**	1.35 $\pm$ 0.08	0.87 $\pm$ 0.06
25 mg/kg	0.59 $\pm$ 0.03**	4.31 $\pm$ 0.27**	0.54 $\pm$ 0.05	0.83 $\pm$ 0.08**	1.33 $\pm$ 0.07	0.86 $\pm$ 0.09

Notes: vs Normal group, \*P < 0.05, \*\*P < 0.01.



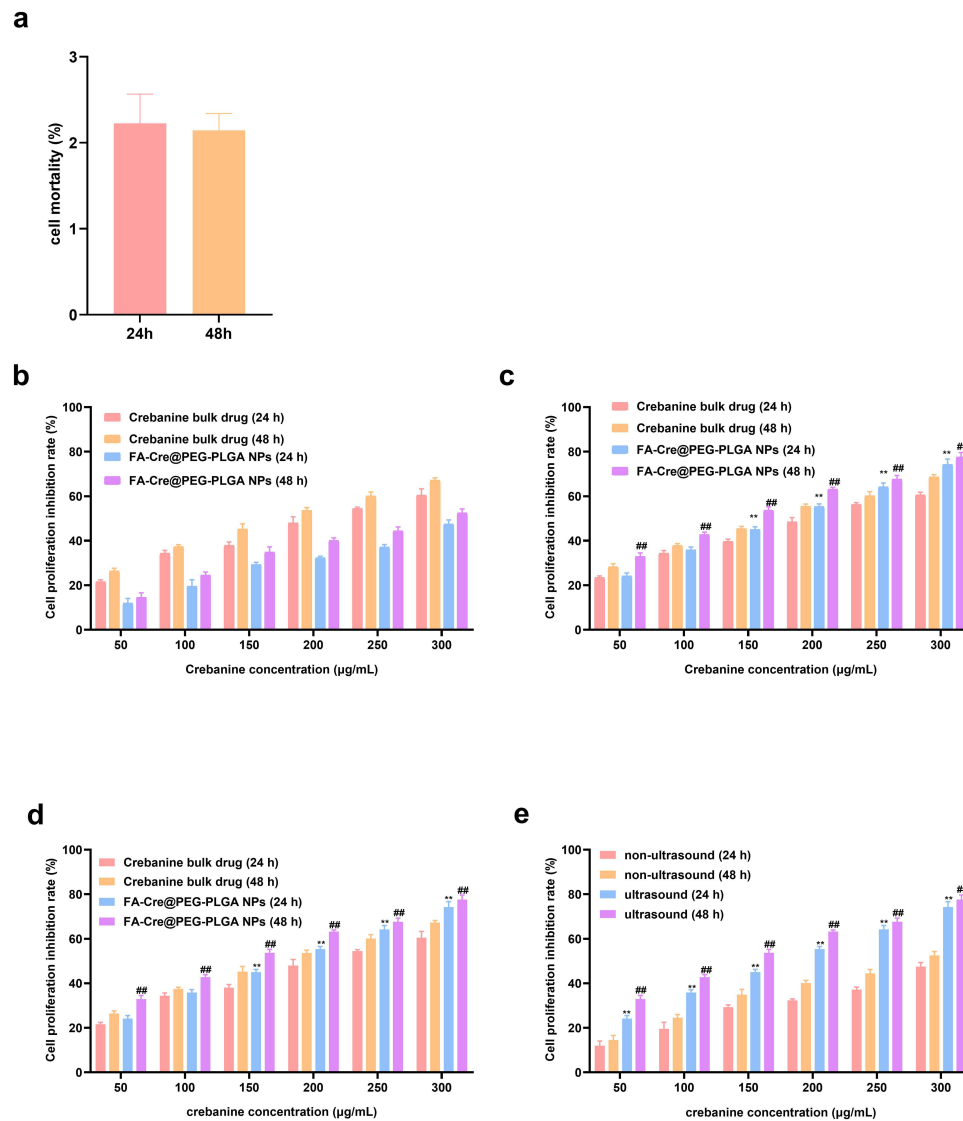


**Figure 7** (a) Cells injury by ultrasound irradiation (b–e) Two Crebanine preparations on the proliferation inhibition rate of H22 cells studies.

**Notes:** (b) Unultrasonic condition, (c) Ultrasonic condition. vs Crebanine bulk drugs, 24 h, \* $P < 0.05$ , \*\* $P < 0.01$ . 48h, # $P < 0.05$ , ### $P < 0.01$ , (d) FA-Cre@PEG-PLGA NPs ultrasound and Crebanine bulk drugs unultrasound 24h, 48h. vs Crebanine bulk drugs unultrasound, 24 h, \* $P < 0.05$ , \*\* $P < 0.01$ . 48h, # $P < 0.05$ , ### $P < 0.01$ , (e) FA-Cre@PEG-PLGA NPs ultrasound and FA-Cre@PEG-PLGA NPs unultrasound 24h, 48h. vs FA-Cre@PEG-PLGA NPs unultrasound, 24 h, \* $P < 0.05$ , \*\* $P < 0.01$ . 48h, # $P < 0.05$ , ### $P < 0.01$ .

resulted in a cell mortality rate below 3% for H22 cells at both 24 and 48 hours (Figure 7a). This indicates that these ultrasound conditions effectively ensure cell safety. Similarly, H22 cells exhibited a cell mortality rate lower than 3% at both time points, suggesting that this particular set of ultrasonic parameters does not cause significant cellular damage and can be considered safe for future experiments.

## Cytotoxicity

The proliferation of H22 cells was dose-dependently inhibited by Crebanine bulk drugs and FA-Cre@PEG-PLGA NPs, with the inhibitory effect increasing as the drug dose increased (Figure 7b). However, in the absence of ultrasound therapy, FA-Cre@PEG-PLGA NPs showed a weaker inhibitory effect on tumor cell proliferation compared to Crebanine bulk drugs at the same concentration and time. Previous findings on the release of FA-Cre@PEG-PLGA NPs indicated slow drug release at 48 hours, suggesting that Crebanine is encapsulated within the nanoparticle. Consequently, the inhibitory rate of tumor cells was comparatively lower than that observed with bulk Crebanine drugs. After 24 and

48 hours of ultrasound treatment, the killing ability of FA-Cre@PEG-PLGA NPs against tumor cells was enhanced (Figure 7c). Following ultrasonic treatment for 24 hours, various concentrations of FA-Cre@PEG-PLGA NPs showed varying degrees of enhancement in their proliferation inhibition rate against H22 cells, and particularly significant differences were observed between concentrations ranging from 150  $\mu\text{g/mL}$  to 300  $\mu\text{g/mL}$  when compared with ultrasound treated Crebanine bulk drugs after 24 hours ( $P < 0.01$ ). Furthermore, after ultrasonic treatment for 48 hours, the inhibitory rate of FA-Cre@PEG-PLGA NPs on cell proliferation continued to increase significantly when compared with Crebanine bulk drugs at concentrations ranging from 50  $\mu\text{g/mL}$  to 300  $\mu\text{g/mL}$  ( $P < 0.01$ ). A comparison between FA-Cre@PEG-PLGA NPs treated with ultrasound at 24 and 48 hours and non-ultrasonic treated Crebanine bulk drugs revealed that FA-Cre@PEG-PLGA NPs had a stronger inhibitory effect on H22 cells than Crebanine bulk drugs. This difference became even more pronounced after a duration of ultrasonic treatment lasting for up to or exceeding 48 hours (Figure 7d,  $P < 0.01$ ). The inhibitory effect of FA-Cre@PEG-PLGA NPs on H22 cells was enhanced when combined with ultrasound, as demonstrated in Figure 7e. Significant differences were observed between FA-Cre@PEG-PLGA NPs after 24 or 48 hours irradiation and those without ultrasound within the concentration range of 50–300  $\mu\text{g/mL}$  ( $P < 0.01$ ). The  $\text{IC}_{50}$  values for Crebanine bulk drugs and FA-Cre@PEG-PLGA NPs without ultrasound at 24 hours were calculated to be  $(210.9 \pm 15.1)$  and  $(322.0 \pm 21.1)$   $\mu\text{g/mL}$ , respectively, while at 48 hours, they were  $(164.4 \pm 9.4)$  and  $(289.5 \pm 19.6)$   $\mu\text{g/mL}$ , respectively. The  $\text{IC}_{50}$  values of Crebanine bulk drugs and FA-Cre@PEG-PLGA NPs after 24 hours ultrasonic irradiation were  $(203.0 \pm 12.0)$  and  $(155.4 \pm 11.1)$   $\mu\text{g/mL}$ , respectively. The  $\text{IC}_{50}$  values of Crebanine bulk drugs and FA-Cre@PEG-PLGA NPs after 48 hours ultrasonic irradiation were  $(157.3 \pm 10.7)$  and  $(117.3 \pm 9.7)$   $\mu\text{g/mL}$ , respectively. The effect of Crebanine bulk drugs on the proliferation inhibition rate of H22 cells before and after ultrasound was not significant. After 24 and 48 hours of ultrasound, the  $\text{IC}_{50}$  of FA-Cre@PEG-PLGA NPs decreased 2.07 times and 2.47 times compared with FA-Cre@PEG-PLGA NPs without ultrasound. Compared with Crebanine bulk drugs, ultrasound decreased by 1.31 times and 1.34 times. After ultrasonic treatment, the proliferation inhibition rate of H22 cells was significantly improved. It was speculated that FA-Cre@PEG-PLGA NPs was broken in the ultrasonic irradiation area, which stimulated the phase transition of nanoparticles for drug release, improved the accumulation of drugs in cells, and increased the proliferation inhibition rate of FA-Cre@PEG-PLGA NPs on H22 cells. The results showed that FA-Cre@PEG-PLGA NPs combined with ultrasonic irradiation enhanced the proliferation inhibition of H22 cells.

## Establishment of Orthotopic Hepatocellular Carcinoma Transplantation Model in Mice

After the modeling procedure, the mice did not exhibit any significant changes and their diet and activity remained within normal parameters. On the third day after surgery, B-ultrasonography was performed to examine the liver of the mice before humanely euthanizing them (Figure 8a and b). Based on the B-ultrasound imaging results and liver appearance, it can be concluded that successful model building was achieved on the third day based on the modeling approach. Subsequently, drug administration experiments were performed on the third day after the model was set up.

## Tumor Targeting Study

Having demonstrated the efficacy of FA-Cre@PEG-PLGA NPs in combination with in vitro ultrasound irradiation, we investigated the biologic distribution behavior of FA-Cre@PEG-PLGA NPs on a mouse model of orthotopic hepatoma transplantation. Figure 8 shows representative fluorescence images of mice at different time points following tail vein injection. All images were acquired using the same imaging setup for ease of comparison. In the FA-Cre@PEG-PLGA NPs group, the fluorescence intensity at the tumor site peaks at 4 hours and gradually decreases over 72 hours. Conversely, in the FA-Cre@PEG-PLGA NPs combined with ultrasonic irradiation group, the fluorescence intensity reached its maximum at 8 hours and remained higher than that observed in the FA-Cre@PEG-PLGA NPs group throughout all time points (Figure 9).

While IVIS spectroscopy has been widely employed to study the biological distribution of tumor-targeting nanocarriers, the evaluation of targeting capabilities has been based primarily on qualitative image analysis rather than quantitative calculations.<sup>41–43</sup> Therefore, we adopt the approach of Liu et al<sup>38</sup> to quantitatively evaluate the tumor targeting effects of both FA-Cre@PEG-PLGA NPs and FA-Cre@PEG-PLGA NPs combined with ultrasound irradiation.



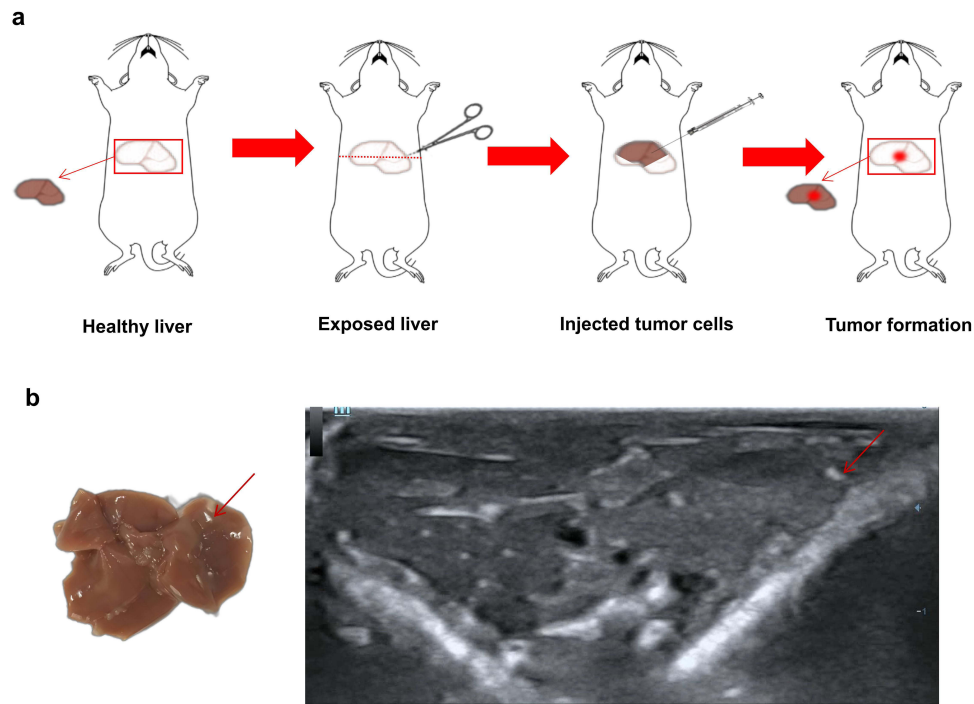


**Figure 8** Establishment of orthotopic hepatocellular carcinoma transplantation model in mice (a) The method of molding (b) The Liver morphology and B-ultrasound figure. **Notes:** The red arrow shows the tumor site.

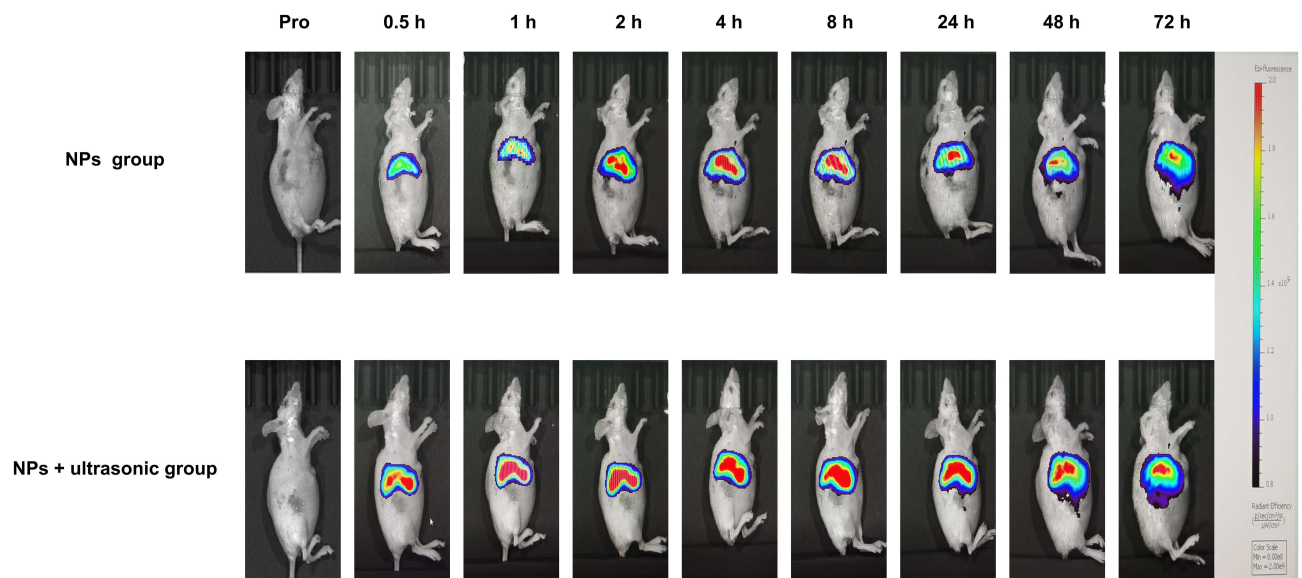


**Figure 9** In vivo FA-Cre@PEG-PLGA NPs fluorescent imaging.

The fluorescence intensity curves for each tumor region are plotted in Figure 10a (At 8, 24, 48 and 72 h,  $P < 0.05$ ). For all imaging time points, FA-Cre@PEG-PLGA NPs combined with ultrasound irradiation exhibit significantly stronger fluorescence than FA-Cre@PEG-PLGA NPs alone. It should be noted, however, that periodically intense tumor fluorescence may be attributed to overall strong fluorescence intensity throughout the body, rather than solely indicating a favorable anti-tumor targeting effect of the nanocarrier.<sup>39</sup> Therefore, we calculate the TTI value to assess whether the fluorescence intensity in the tumor region genuinely reflects the drug accumulation inside the tumor, making the TTI percentage proportional to the tumor targeting capability of the nanocarrier. Nevertheless, since TTI values can only

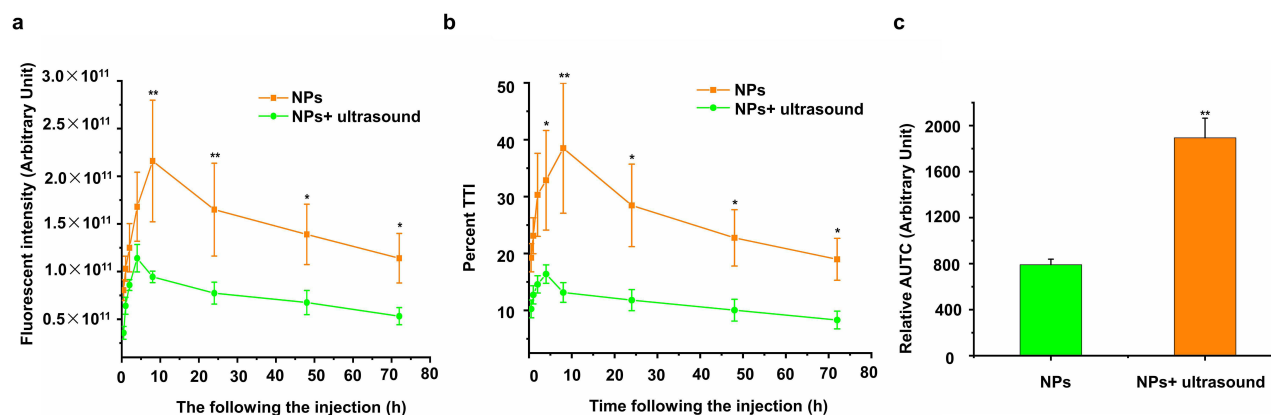


**Figure 10** Quantitative analysis of in vivo FA-Cre@PEG-PLGA NPs fluorescence imaging (mean  $\pm$  SD, n = 5).

**Notes:** (a) The DiR fluorescence intensity curves of the tumor regions in the mice. (b) The tumor-targeting index (TTI) curves of different groups. (c) The relative area under the TTI-time curve (AUTC) of each group. In figures (a–c), vs NPs group, \*P < 0.05, \*\*P < 0.01.

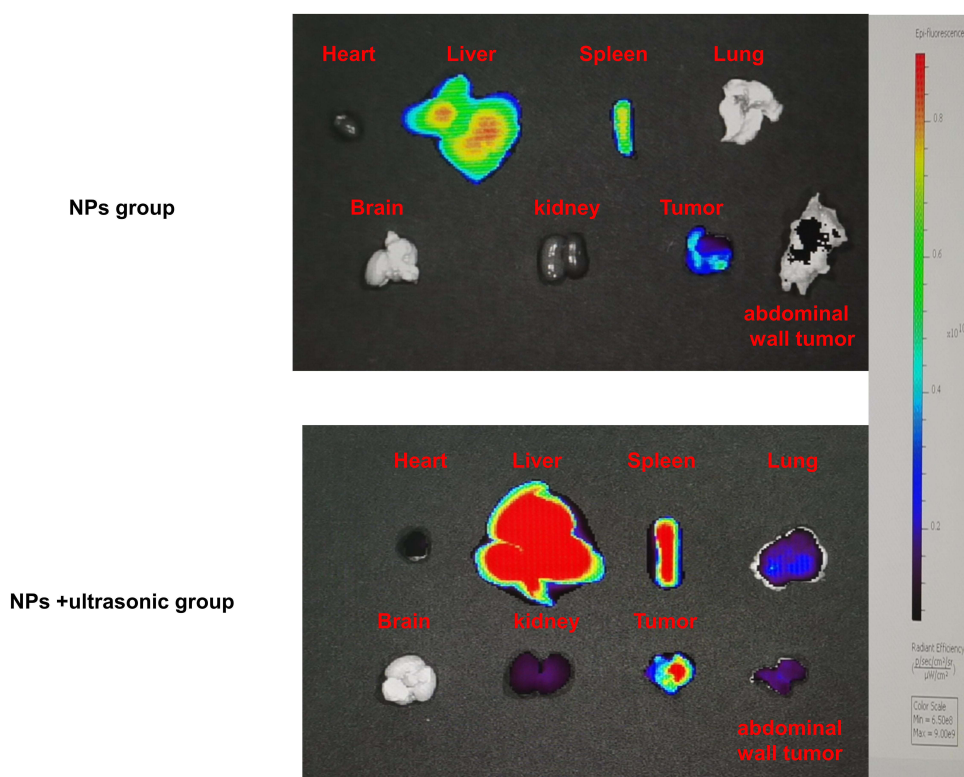


**Figure 11** Ex vivo FA-Cre@PEG-PLGA NPs fluorescent imaging of tumors and organs/tissues from the mice.

indicate tumor targeting ability at a specific time point, we additionally computed AUTC as an indicator representing the overall effectiveness of nanocarriers' tumor targeting capability (Figure 10b, at 4, 8, 24, 48 and 72 h, P < 0.05). In agreement with our findings in Figure 9, the average TTI values for FA-Cre@PEG-PLGA NPs combined with ultrasound irradiation are consistently higher than those for FA-Cre@PEG-PLGA NPs across all evaluated time points. Moreover, results from calculating TTI-Area under Time Curve (AUTC) demonstrated that AUTC for FA-Cre@PEG-PLGA NPs combined with ultrasound irradiation was significantly greater than that observed for FA-Cre@PEG-PLGA NPs alone (Figure 10c, P < 0.01), thereby indicating superior overall efficacy in terms of tumor targeting.

Representative fluorescence images of different groups of tumors, abdominal wall tumors and tissues are shown in Figure 11. Under the same imaging setup, the fluorescence intensity of tumor and abdominal wall tumors in FA-Cre

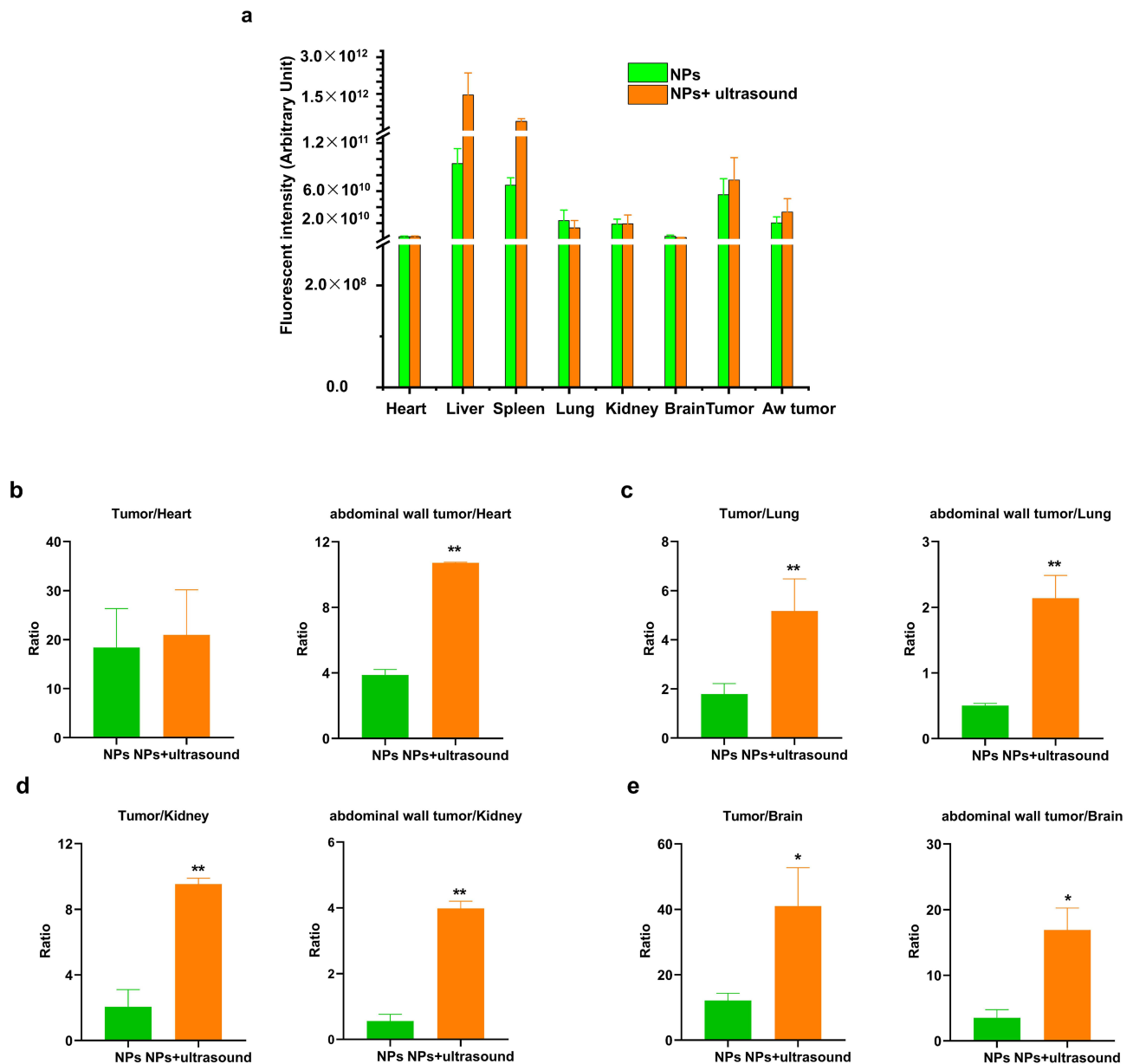


**Figure 12** Quantitative analysis of ex vivo NIR fluorescence imaging (mean  $\pm$  SD,  $n = 5$ ).

**Notes:** (a) The DiR fluorescence intensity of tumors/abdominal wall tumor and organs/tissues of the mice. (b–e) Fluorescence intensity ratios of tumor/abdominal wall tumor to Heart (b), Lung (c), Kidney (d), and Brain (e). In figures (b–e), Left: Fluorescence intensity ratios of tumor to organs/tissues, Right: Fluorescence intensity ratios of abdominal wall tumor to organs/tissues. In figure (a), Aw Tumor stands for abdominal wall tumor. vs NPs group, \* $P < 0.05$ , \*\* $P < 0.01$ .

@PEG-PLGA NPs combined with ultrasound irradiation is significantly stronger than in FA-Cre@PEG-PLGA NPs, in agreement with in vivo imaging results. To further compare FA-Cre@PEG-PLGA NPs with FA-Cre@PEG-PLGA NPs combined with ultrasound irradiation, we quantified the fluorescence intensity for each tumor, abdominal wall tumor and tissue. The fluorescence intensity of tumors in both groups was higher than that in other tissues (except liver and spleen). Moreover, the results from the FA-Cre@PEG-PLGA NPs combined with ultrasonic irradiation group were significantly superior to those from the FA-Cre@PEG-PLGA NPs group (Figure 12a). The fluorescence intensity ratios of tumor/abdominal wall tumor and heart/lung/kidney/brain were higher in the FA-Cre@PEG-PLGA NPs combined with ultrasound irradiation group compared to those in the FA-Cre@PEG-PLGA NPs group (Figure 12b–e). These findings indicate that the combination of FA-Cre@PEG-PLGA NPs preparation with ultrasound irradiation exhibits excellent tumor targeting properties.

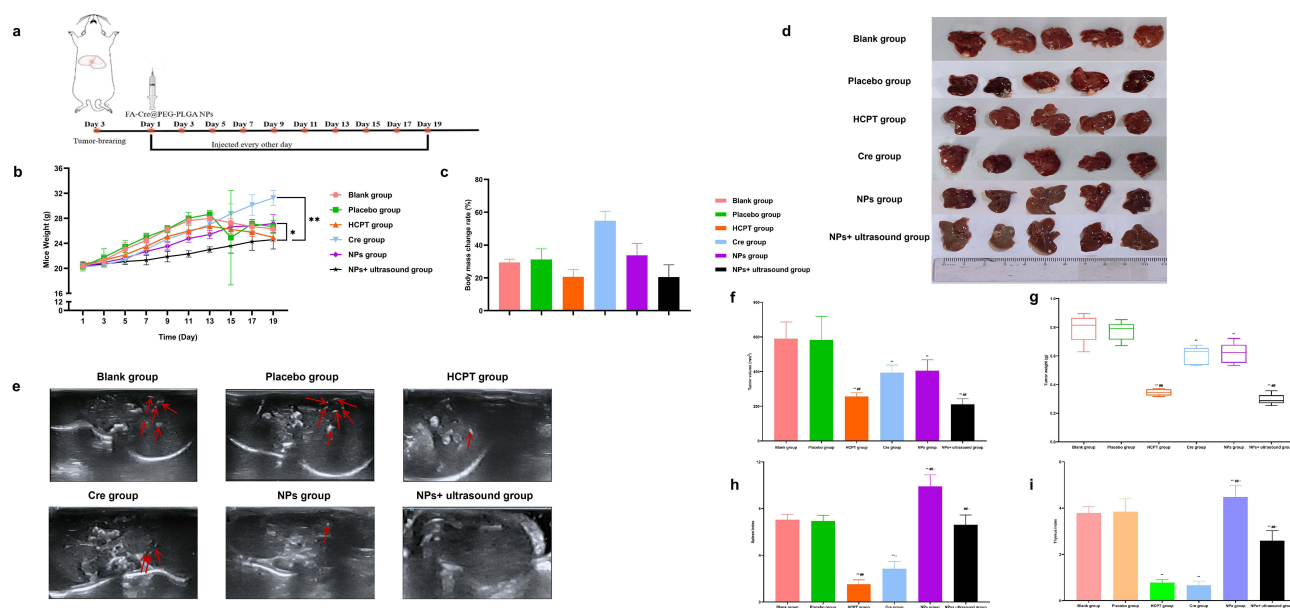


**Figure 13** (a) Schematic of treatment schedule. (b) weight growth of mice in each group.(c) body mass change rate. (d) Tumor of mice in each group after administration. (e) B-ultrasound imaging. (f) Tumor volume. (g) Tumor weight. (h) Spleen index.(i) Thymus index. **Notes:** (b) vs blank group, \*P < 0.05, \*\*P < 0.01. (c) The red arrow shows the tumor site. (f-i), vs blank group, \*P < 0.05, \*\*P < 0.01, vs Cre group, #P < 0.05, ##P < 0.01, vs HCPT group, P < 0.05, P < 0.01.

## Antitumor Efficacy and Biocompatibility of FA-Cre@PEG-PLGA NPs

A situ model of liver cancer was administered to validate the therapeutic efficacy (Figure 13a). Initially, we monitored the body mass of the mice in each group every other day. No mortality was observed in any of the mice across all groups throughout the course of the drug treatment. Mice in both the blank and placebo groups had a peak in body mass at the 13th day, after which it showed a decreasing trend. The mice showed lethargy and general deterioration, resulting in reduced food intake and reduced body mass. In turn, the mental states of the mice in the other groups appeared to be more active than those in the blank and placebo groups. The group that received hydroxycamptothecin injection also experienced a reduction in the body mass of the mice, suggesting that the higher toxicity of the hydroxycamptothecin injection was responsible for the decrease in body mass (Figure 13b). The rate of weight change in the mice subjected to FA-Cre@PEG-PLGA NPs combined with ultrasound irradiation remained relatively stable compared to the other groups, suggesting that nanoparticle formulation using Crebanine with combined ultrasonic irradiation resulted in lower toxicity and minimal impact on mice (Figure 13c).

According to the B-ultrasound imaging and anatomical results, the FA-Cre@PEG-PLGA NPs combined with ultrasound irradiation group exhibited a lower number of metastatic tumor nodules (indicated by red arrows) compared to the blank group and placebo group (Figure 13d and e). The incidence of severe abdominal adhesion in the control group and placebo group exceeded 85%, while the degree of abdominal adhesion was significantly reduced in other treatment groups. Among them, the FA-Cre@PEG-PLGA NPs combined with ultrasound irradiation group demonstrated the most effective outcome, with a complete absence of severe abdominal adhesion (Table 5). Additionally, noticeable

**Table 5** Comparison of Abdominal Adhesion Grade Among the Four Groups [n=7]

Adhesion Grade	Blank Group	Placebo Group	HCPT Group	Cre Group	NPs Group	NPs+ Ultrasound Group
Lv.0	0%	0%	28.6%	0%	0%	42.9%
Lv. 2160	0%	0%	42.9%	28.6%	28.6%	42.9%
Lv. 2161	14.3%	14.3%	14.3%	57.1%	42.9%	14.3%
Lv. 2162	28.6%	14.3%	14.3%	14.3%	28.6%	0%
Lv. 2163	57.1%	71.4%	0%	0%	0%	0%



blood ascites were observed in both the control group and placebo group, indicating extensive tumor infiltration. In turn, mice treated with FA-Cre@PEG-PLGA NPs combined with ultrasound irradiation showed a significant reduction in ascites occurrence rate and volume. The ascites volume for the blank group and placebo group was measured at  $(10.357 \pm 1.314)$  mL and  $(10.000 \pm 1.414)$  mL, respectively. For hydroxycamptothecin injection treated mice, it was recorded as  $(5.333 \pm 2.160)$  mL, whereas for those receiving original drug treatment it was noted as  $(8.167 \pm 0.075)$  mL, finally for FA-Cre@PEG-PLGA NPs it amounted to  $(5.667 \pm 1.211)$  mL. However, when FA-Cre@PEG-PLGA NPs combined with ultrasound irradiation, this volume decreased significantly to only  $(2.250 \pm 1.258)$  mL compared to other groups ( $P < 0.01$ ). The rate of abdominal wall tumors was significantly reduced in each administration group compared to the blank and placebo groups. The weight of abdominal wall tumors in the blank group and placebo group was  $(1.833 \pm 0.473)$  g and  $(1.894 \pm 0.468)$  g, respectively. In the hydroxycamptothecin injection group, the weight of abdominal wall tumors was  $(0.382 \pm 0.153)$  g. The Crebanine bulk drugs group had an abdominal wall tumor weight of  $(0.814 \pm 0.205)$  g. The FA-Cre@PEG-PLGA NPs group had an abdominal wall tumor weight of  $(0.439 \pm 0.118)$  g. Compared to other groups, the combination treatment of FA-Cre@PEG-PLGA NPs and ultrasound irradiation significantly reduced the weight of abdominal wall tumors to  $(0.128 \pm 0.040)$  g ( $P < 0.05$ ). FA-Cre@PEG-PLGA NPs combined with ultrasound irradiation can significantly reduce the occurrence rate and weight of abdominal wall tumors. Compared with IVIS imaging results (Figure 12b–d), FA-Cre@PEG-PLGA NPs combined with ultrasound irradiation have better targeting efficiency for abdominal wall tumors than heart, lung, kidney and brain tissues. These findings indicate that FA-Cre@PEG-PLGA NPs in combination with ultrasonic irradiation have a higher effective therapeutic effect (Table 6). The mice were euthanized 24 hours after the final treatment, and the final tumor volume and weight were reassessed by surgical resection. Of these, tumors in the FA-Cre@PEG-PLGA NPs combined with ultrasound irradiation group showed the most significant reduction compared to the blank group. Although other treatment groups also showed a decrease in tumor size, it was not as substantial as observed in the FA-Cre@PEG-PLGA NPs combined with ultrasound irradiation group. The TCI value of FA-Cre@PEG-PLGA NPs combined with ultrasonic irradiation group reached 63.94%, which was 2.86 times, 1.68 times, and 1.26 times higher than that in the FA-Cre@PEG-PLGA NPs group, Crebanine bulk drugs group, and HCPT injection group, respectively (Figure 13f and g). In summary, these results suggest that the combination of FA-Cre@PEG-PLGA NPs with ultrasound irradiation effectively inhibits tumor cell proliferation.

In this study, we not only assessed efficacy but also investigated the biosecurity of FA-Cre@PEG-PLGA NPs in combination with ultrasound irradiation. The safety of this treatment has potential translational clinical implications. First, to determine whether FA-Cre@PEG-PLGA NPs exhibit any toxic effects on immune organs, we measured spleen and thymus indices. The results demonstrated that both hydroxycamptothecin injection group and Crebanine bulk drug group exhibited significantly lower spleen and thymus indexes compared to the blank group, indicating certain toxic effects on these organs ( $P < 0.01$ ). Conversely, the spleen and thymus indexes in the FA-Cre@PEG-PLGA NPs group were significantly higher than those in the blank group ( $P < 0.01$ ). When combined with ultrasound irradiation, FA-Cre@PEG-PLGA NPs showed a slight increase or decrease in spleen and thymus indices compared to the blank population. We hypothesized that both FA-Cre@PEG-PLGA NPs alone and when combined with ultrasound irradiation may enhance nonspecific immunity in mice (Figure 13h and i). ALT, AST, BUN, and CREA are sensitive marker enzymes that reflect

**Table 6** Comparison of Tumor Status of Mice in Each Group (n = 7)

Group	Ascites Occurrence Rate (%)	Ascites Volume(mL)	Abdominal Wall Tumor Occurrence Rate (%)	Abdominal Wall Tumor Weight(g)
Blank group	100%	10.357±1.314	100%	1.833±0.473
Placebo group	100%	10.000±1.414	100%	1.894±0.468
HCPT group	85.7%	5.333±2.160 <sup>**#</sup>	57.1%	0.382±0.153 <sup>***</sup>
Cre group	100%	8.167±0.0753 <sup>*</sup>	71.4%	0.814±0.205 <sup>**</sup>
NPs group	85.7%	5.667±1.211 <sup>**</sup>	71.4%	0.439±0.118 <sup>***</sup>
NPs+ ultrasound group	57.1%	2.250±1.258 <sup>****</sup>	57.1%	0.128±0.040 <sup>****</sup>

**Notes:** vs blank group, \* $P < 0.05$ , \*\* $P < 0.01$ , vs Cre group, # $P < 0.05$ , ## $P < 0.01$ , vs HCPT group,  $P < 0.05$ ,  $^{\dagger}P < 0.01$ .



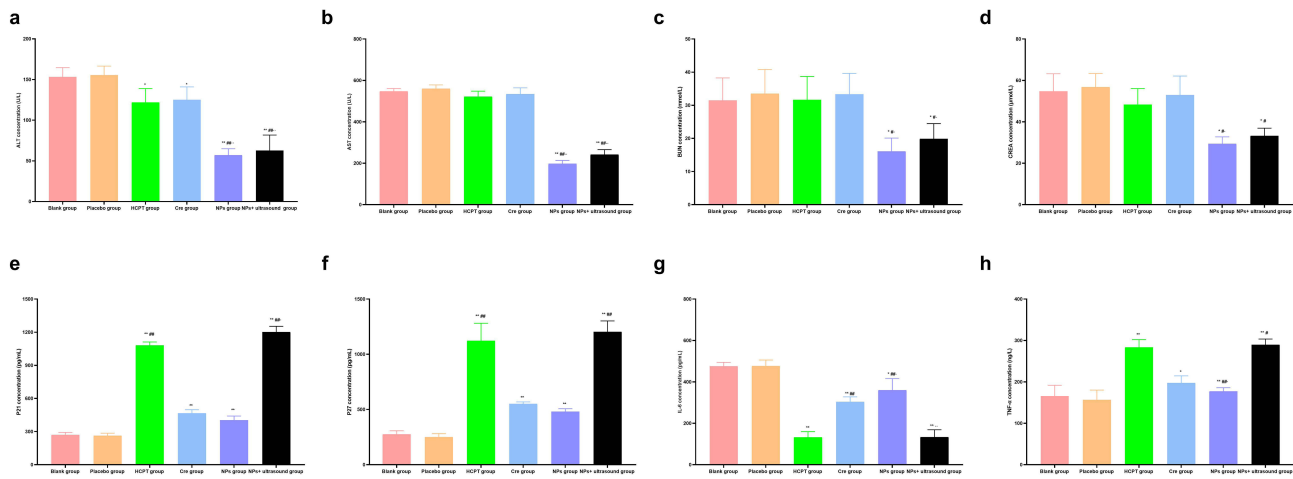


**Figure 14** (a) ALT. (b) AST. (c) BUN. (d) CREA. (e) P21. (f) P27. (g) TNF- $\alpha$ . (h) IL-6 levels of mice in each group.  
**Notes:** (a–h) vs blank group, \* $P < 0.05$ , \*\* $P < 0.01$ . vs Cre group,  $^{\#}P < 0.05$ ,  $^{\#\#}P < 0.01$ . vs HCPT group,  $^{\Delta}P < 0.05$ ,  $^{\Delta\Delta}P < 0.01$ .

liver and kidney injury, and their levels can partially indicate the extent of damage to liver and kidney cells. The results of this trial demonstrated that all treatment groups showed varying levels of reduction in ALT, AST, BUN and CREA levels compared to the blank and placebo groups. Moreover, when compared with the hydroxycamptothecin injection and Crebanine bulk drugs group, both the FA-Cre@PEG-PLGA NPs group and the FA-Cre@PEG-PLGA NPs combined with ultrasonic irradiation group showed a significant decrease in ALT, AST, BUN, and CREA levels ( $P < 0.01$ ) (Figure 14a–d). These findings suggest that the injection of hydroxycamptothecin injection and the Crebanine bulk drug resulted in severe impairment of liver and kidney function in mice. However, FA-Cre@PEG-PLGA NPs showed some protective effects on the liver and kidneys of mice with in-situ liver cancer. Additionally, ELISA analysis was conducted to determine serum levels of P21, P27, TNF- $\alpha$  and IL-6 in all groups of mice. The results also indicated that combination therapy involving FA-Cre@PEG-PLGA NPs along with ultrasound irradiation significantly increased P21 and P27 levels while significantly decreasing TNF- $\alpha$  and IL-6 levels ( $P < 0.05$ ) (Figure 14e–h). Finally, histological tests were performed on the liver and kidneys of each group of mice using HE stain. Hyperplastic and cancerous nodules were observed in the liver cells of both the blank and placebo groups of mice. Tumor cells exhibit tight alignment, deep nuclear staining, and infiltration of inflammatory cells. In the FA-Cre@PEG-PLGA NPs group combined with ultrasound irradiation, significant improvement was observed in the pathological structure, along with a notable reduction in inflammatory cells and cancer cells (Figure 15). The renal glomeruli and renal tubules showed normal structural characteristics without any discernible differences compared to the control group when FA-Cre@PEG-PLGA NPs

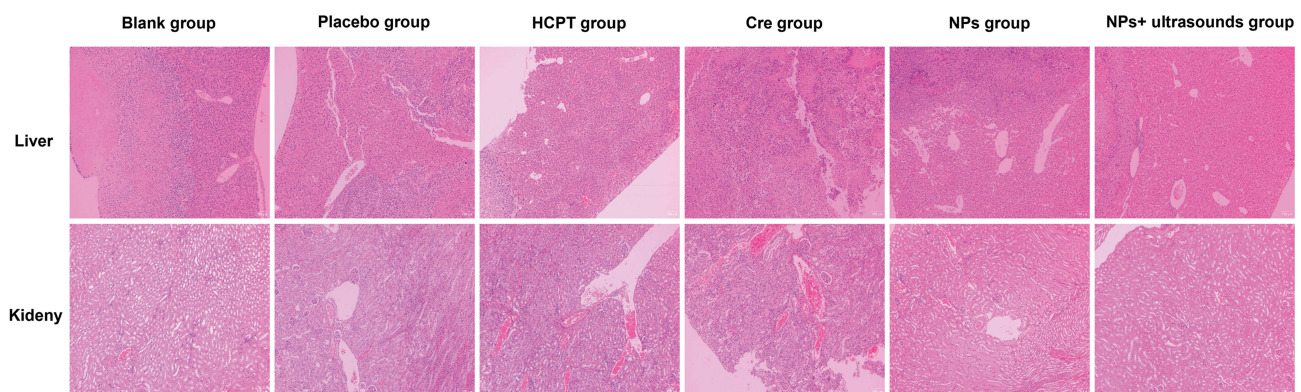


**Figure 15** HE staining images of liver and kidney.

were combined with ultrasound irradiation (Figure 15). No significant pathological changes such as oedema or necrosis were observed.

In conclusion, these results demonstrate the efficacy and safety of combining FA-Cre@PEG-PLGA NPs with ultrasound irradiation to significantly enhance the therapeutic effect on in-situ hepatocellular carcinoma while promoting immune activity. This combination strategy provides an active physical dual targeting effect that facilitates the better release of Crebanine at the tumor site for improved therapeutic outcomes.

## Discussion

Liver cancer has a high incidence and mortality rate, making it a malignancy. Although commonly used in clinical treatment, chemotherapy still has drawbacks such as lack of targeting and significant side effects. While inhibiting the growth of liver cancer cells, it also causes damage to normal cells. To overcome these limitations in the clinical treatment of liver cancer, there is a pressing need to develop drug delivery systems for early detection and targeted treatment.

In recent years, precision medicine has paved the way for the widespread use of functional nanodrug delivery systems in liver cancer research.<sup>44</sup> These systems incorporate ultrasound imaging, drug delivery mechanisms, and therapeutic genes. To enhance their accumulation at tumor sites, nano drug delivery systems can be modified with sugar groups, folic acid (FA), or antibodies to achieve active targeting effects and improve anti-liver cancer efficacy.<sup>45,46</sup> In this study, we have designed a nanocarrier that integrates active targeting, ultrasonic physical targeting, and fluorescence localization, and verified its efficacy in the treatment of liver cancer, laying a foundation for the early diagnosis and treatment of liver cancer.

After the intravenous injection of Crebanine injection, it was rapidly and widely distributed in rabbits, with a half-life time of less than 1 hour.<sup>47</sup> In this study, the pharmacokinetic results of FA-Cre@PEG-PLGA NPs and Crebanine bulk drug after intravenous administration in rats demonstrated that the elimination phase half-life time in vivo was prolonged, reaching more than 2 hours for both. Furthermore, the in vivo AUC of FA-Cre@PEG-PLGA NPs was significantly higher than that of Crebanine bulk drug, indicating that the formulation of Crebanine nanoparticles could enhance bioavailability in vivo. The in vivo retention time of drugs MRT and elimination-phase half-life time of FA-Cre@PEG-PLGA NPs were significantly higher than those of Crebanine bulk drug, while the distribution-phase half-life time and total body clearance were lower than those of Crebanine bulk drug. It was confirmed that FA-Cre@PEG-PLGA NPs exhibited the characteristics of faster distribution, longer retention time, and prolonged elimination in rats.

PEG-PLGA polymer nanocarriers are extensively utilized in drug delivery due to their excellent biocompatibility. We have developed folic acid-modified Crebanine polyethylene glycol-poly(lactic acid) copolymer nanoparticles, namely FA-Cre@PEG-PLGA NPs. In this investigation, we monitored the pharmacokinetics of FA-Cre@PEG-PLGA NPs. The outcomes demonstrated that, in contrast to Crebanine, FA-Cre@PEG-PLGA NPs exhibited a certain sustained-release effect. It is hypothesized that this slow-release effect might stem from the shell material PLGA, which has a sluggish degradation rate in vivo, thereby prolonging its action duration. These findings are in line with previous in vitro release experiments and further validate that FA-Cre@PEG-PLGA NPs can notably enhance the bioavailability of Crebanine. Ce, Si, Re, and Te were employed in tissue distribution experiments to further explore the targeting capability of FA-Cre@PEG-PLGA NPs. The results imply that FA-Cre@PEG-PLGA NPs have a specific liver-targeted accumulation effect.

Ultrasound targeted microvesicle technology serves a dual purpose by enabling simultaneous diagnosis and treatment. Drug-loaded microbubbles can precisely target tumor sites and release drugs under ultrasound while concurrently mediating tumor cell apoptosis and growth inhibition, thereby achieving targeted anti-tumor effects. Among the ultrasonic diagnostic parameters, frequency and mechanical parameters are the key factors influencing ultrasonic cavitation and facilitating the phase transition of nanoparticles.<sup>48</sup> In accordance with FDA regulations, the MI limit set for diagnostic ultrasound is 1.9. The higher the frequency or the lower the peak negative pressure, the smaller the MI value and the lower the likelihood of a cavitation effect.<sup>49</sup> Recent studies have demonstrated that when MI is 0.3, ultrasonic energy can induce transient cavitation of microvesicles in blood vessels without causing adverse reactions resulting from high peak negative pressure.<sup>50</sup> Additionally, within the ultrasonic irradiation range of 1.8–12 MHz, microbubbles can exert a strong cavitation effect.<sup>51</sup>

Non-invasive, safe and effective low-intensity ultrasound was used in this study. In combination with previous studies, higher frequency and lower mechanical index were chosen to achieve in vitro ultrasonic demulsification of nanoparticles.<sup>52</sup> Minimal cell damage and a mortality rate of less than 3% were observed after ultrasound irradiation, indicating that it is suitable as a source of cell ultrasound in vitro. The results of the CCK-8 experiment confirm that FA-Cre@PEG-PLGA NPs in combination with ultrasound irradiation exhibit an enhanced inhibitory effect on tumor cell proliferation. Presumably, ultrasound irradiation not only ruptures microvesicles but also enhances cell membrane permeability and promotes endocytosis, thus improving drug uptake by cells and thus enhancing the therapeutic efficacy of the drug, as supported by previous studies of uptake in liver cancer Bell-7402 cells.<sup>36</sup>

The establishment of animal models is of vital significance for the success of the experiments, offering insights into the pathogenesis of the disease and the effects of drug treatment. Previous studies have demonstrated that FA-Cre@PEG-PLGA NPs in combination with ultrasound irradiation exhibit a favorable anti-tumor effect in the treatment of subcutaneous liver cancer in mice and display a certain dose dependence.<sup>53</sup> Therefore, this study aims to further investigate the therapeutic effect and biological distribution behavior of liver cancer in mice under previous studies optimal treatment dose. By comparing factors such as weight change, tumor weight, tumor volume, B-ultrasound imaging, ascites volume, abdominal wall tumor weight, spleen and thymus index, ALT, AST, BUN, CREA, P21, and other indicators including P27, TNF- $\alpha$ , and IL-6 indexes, the results once again confirmed that FA-Cre@PEG-PLGA NPs combined with ultrasonic irradiation exerted specific anti-tumor effects while causing minimal damage to immune organs, liver and kidney tissues. It has been proposed that the cavitation effect induced by ultrasound irradiation plays a crucial role in enhancing anti-tumor therapy.

The present study, however, exhibits certain limitations, including suboptimal active targeting efficiency of the nanoparticles and insufficient optimization of the ultrasound parameters. Consequently, future investigations will focus on refining the nanoparticle preparation scheme for enhanced targeted therapy of liver cancer.

## Conclusion and Future Perspective

In conclusion, FA-Cre@PEG-PLGA NPs demonstrate significant efficacy in tumor inhibition and exhibit a favorable safety profile. It is anticipated that the combination of FA-Cre@PEG-PLGA NPs with ultrasound irradiation will emerge as a novel strategy for the diagnosis and treatment of liver cancer.

## Acknowledgments

This study was conducted by the Open and Shared Public Science and Technology Service Platform of Traditional Chinese Medicine Science and Technology Resources in Yunnan which provide instrument use and technical support.

## Funding

The funding for this work is provided by the Project of Yunnan Provincial Science and Technology Department-Applied Basic Research Joint Special Funds of Chinese Medicine (202001AZ070001-008). Major Scientific and Technological Projects for Biomedical Industry of Yunnan Provincial Science and Technology Department (202002AA100007). Yunnan Provincial Science and Technology Talent Platform (202105AG070012). Yunnan Provincial Key Laboratory of Dai Medicine and Yi Medicine (202210ZD2207, 202210SS2205, 202210SS2206). Key Discipline of Twelfth Five-Year Plan of State Administration of Traditional Chinese Medicine-Dai Pharmacy. Yunnan Provincial Department of Education Scientific Research Fund Project (2024Y345).

## Disclosure

The authors report no conflicts of interest in this work.

## References

1. Siegel RL, Miller KD, Fuchs HE, et al. Cancer statistics, 2022. *CA Cancer J Clin.* 2022;72(1):7–33. doi:10.3322/caac.21708
2. Frick C, Rungay H, Vignat J, et al. Quantitative estimates of preventable and treatable deaths from 36 cancers worldwide: a population-based study. *Lancet Glob Health.* 2023;11(11):e1700–e1712. doi:10.1016/S2214-109X(23)00406-0

3. Nagaraju GP, Dariya B, Kasa P, et al. Epigenetics in hepatocellular carcinoma. *Semin Cancer Biol.* 2022;86:622–632. doi:10.1016/j.semcancer.2021.07.017
4. Wen N, Cai Y, Li F, et al. The clinical management of hepatocellular carcinoma worldwide: a concise review and comparison of current guidelines: 2022 update. *Biosci Trends.* 2022;16(1):20–30. doi:10.5582/bst.2022.01061
5. Sim HW, Knox J. Hepatocellular carcinoma in the era of immunotherapy. *Curr Probl Cancer.* 2018;42(1):40–48. doi:10.1016/j.currprobcancer.2017.10.007
6. Alawiyia B, Constantinou C. Hepatocellular carcinoma: a narrative review on current knowledge and future prospects. *Curr Treat Options Oncol.* 2023;24(7):711–724. doi:10.1007/s11864-023-01098-9
7. Vyas M, Zhang X. Hepatocellular carcinoma: role of pathology in the era of precision medicine. *Clin Liver Dis.* 2020;24(4):591–610. doi:10.1016/j.cld.2020.07.010
8. Xiong S, Liu W. Role of metformin in the diagnosis, prevention, and treatment of hepatocellular carcinoma. *Zhong Nan Da Xue Xue Bao Yi Xue Ban.* 2022;47(3):364–373. [English, Chinese]. doi:10.11817/j.issn.1672-7347.2022.210118
9. Wang Y, Yin Z, Gao L, et al. Lipid nanoparticles-based therapy in liver metastasis management: from tumor cell-directed strategy to liver microenvironment-directed strategy. *Int J Nanomed.* 2023;18:2939–2954. doi:10.2147/IJN.S402821
10. Anwanwan D, Singh SK, Singh S, et al. Challenges in liver cancer and possible treatment approaches. *Biochim Biophys Acta Rev Cancer.* 2020;1873(1):188314. doi:10.1016/j.bbcan.2019.188314
11. Wang Y, Chen M, Yu H, et al. The role and mechanisms of action of natural compounds in the prevention and treatment of cancer and cancer metastasis. *Front Biosci.* 2022;27(6):192. doi:10.31083/j.fbl2706192
12. He F, Wen N, Xiao D, et al. Aptamer-based targeted drug delivery systems: current potential and challenges. *Curr Med Chem.* 2020;27(13):2189–2219. doi:10.2174/0929867325666181008142831
13. Wang K, Shen R, Meng T, et al. Nano-drug delivery systems based on different targeting mechanisms in the targeted therapy of colorectal cancer. *Molecules.* 2022;27(9):2981. doi:10.3390/molecules27092981
14. Zhou L, Li Y, Liang Q, et al. Combination therapy based on targeted nano drug co-delivery systems for liver fibrosis treatment: a review. *J Drug Target.* 2022;30(6):577–588. doi:10.1080/1061186X.2022.2044485
15. Ruman U, Fakurazi S, Masarudin MJ, et al. Nanocarrier-based therapeutics and theranostics drug delivery systems for next generation of liver cancer nanodrug modalities. *Int J Nanomed.* 2020;15:1437–1456. doi:10.2147/IJN.S236927
16. Loujin H, Evans James C, Christine A. Overcoming the road blocks: advancement of block copolymer micelles for cancer therapy in the clinic. *Mol Pharm.* 2017;14(8):2503–2517. doi:10.1021/acs.molpharmaceut.7b00188
17. Cheng K, Zhou J, Zhao Y, et al. pH-responsive and CD44-targeting polymer micelles based on CD44p-conjugated amphiphilic block copolymer PEG-*b*-HES-*b*-PLA for delivery of emodin to breast cancer cells. *Nanotechnology.* 2022;33(27):1–12. doi:10.1088/1361-6528/ac5f9a
18. Mohamed MA, Singh A, Prasad PN, et al. Well-defined pH-sensitive self-assembled triblock copolymer-based crosslinked micelles for efficient cancer chemotherapy. *Molecules.* 2022;27(23):8153. doi:10.3390/molecules27238153
19. Clarysse M, Accarie A, Panisello-Roselló A, et al. Intravenous polyethylene glycol alleviates intestinal ischemia-reperfusion injury in a rodent model. *Int J Mol Sci.* 2023;24(13):10775. doi:10.3390/ijms241310775
20. Nie X, Liu Y, Li M, et al. SP94 peptide-functionalized PEG-PLGA nanoparticle loading with cryptotanshinone for targeting therapy of hepatocellular carcinoma. *AAPS Pharm Sci Tech.* 2020;21(4):124. doi:10.1208/s12249-020-01655-7
21. Sun F, Sun X, Wang H, et al. Application of 3D-printed, PLGA-based scaffolds in bone tissue engineering. *Int J Mol Sci.* 2022;23(10):5831. doi:10.3390/ijms23105831
22. Li Y, Wang C, Deng X, et al. Preparation of thifluzamide polylactic acid glycolic acid copolymer microspheres and its effect on the growth of cucumber seedlings. *Int J Mol Sci.* 2023;24(12):10121. doi:10.3390/ijms241210121
23. Tanna V, Vora A, Shah P, et al. PLGA nanoparticles based mucoadhesive nasal in situ gel for enhanced brain delivery of topiramate. *AAPS Pharm Sci Tech.* 2024;25(7):205. doi:10.1208/s12249-024-02917-4
24. Jo S, Roh S, Shim J, et al. Modulating the thermoresponsive characteristics of PLGA-PEG-PLGA hydrogels via manipulation of PLGA monomer sequences. *Biomacromolecules.* 2024;25(8):5374–5386. doi:10.1021/acs.biomac.4c00817
25. Alharthi S, Alavi SZ, Nisa MU, et al. Developing engineered nano-immunopotentiators for the stimulation of dendritic cells and inhibition and prevention of melanoma. *Pharm Res.* 2024;41(6):1163–1181. doi:10.1007/s11095-024-03722-1
26. Narmani A, Rezvani M, Farhood B, et al. Folic acid functionalized nanoparticles as pharmaceutical carriers in drug delivery systems. *Drug Dev Res.* 2019;80(4):404–424. doi:10.1002/ddr.21545
27. Hao J, Tong T, Jin K, et al. Folic acid-functionalized drug delivery platform of resveratrol based on pluronic 127/D- $\alpha$ -tocopheryl polyethylene glycol 1000 succinate mixed micelles. *Int J Nanomed.* 2017;12:2279–2292. doi:10.2147/IJN.S130094
28. Mi X, Hu M, Dong M, et al. Folic acid decorated zeolitic imidazolate framework (ZIF-8) loaded with baicalin as a nano-drug delivery system for breast cancer therapy. *Int J Nanomed.* 2021;16:8337–8352. doi:10.2147/IJN.S340764
29. Deng H, Wang Y, Zhou Y, et al. In vitro and in vivo evaluation of folic acid modified DOX-loaded <sup>32</sup>P-nHA nanoparticles in prostate cancer therapy. *Int J Nanomed.* 2023;18:2003–2015. doi:10.2147/IJN.S403887
30. Wang Y, Lan M, Shen D, et al. Targeted nanobubbles carrying indocyanine green for ultrasound, photoacoustic and fluorescence imaging of prostate cancer. *Int J Nanomed.* 2020;15:4289–4309. doi:10.2147/IJN.S243548
31. Gao H, Wang Z, Tan M, et al. pH-responsive nanoparticles for enhanced antitumor activity by high-intensity focused ultrasound therapy combined with sonodynamic therapy. *Int J Nanomed.* 2022;17:333–350. doi:10.2147/IJN.S336632
32. He K, Ran H, Su Z, et al. Perfluorohexane-encapsulated fullerene nanospheres for dual-modality US/CT imaging and synergistic high-intensity focused ultrasound ablation. *Int J Nanomed.* 2019;14:519–529. doi:10.2147/IJN.S184579
33. Li H, Shi S, Wu M, et al. iRGD peptide-mediated liposomal nanoparticles with photoacoustic/ultrasound dual-modality imaging for precision theranostics against hepatocellular carcinoma. *Int J Nanomed.* 2021;16:6455–6475. doi:10.2147/IJN.S325891
34. Jia X, Cai X, Chen Y, et al. Perfluoropentane-encapsulated hollow mesoporous Prussian blue nanocubes for activated ultrasound imaging and photothermal therapy of cancer. *ACS Appl Mater Interfaces.* 2015;7(8):4579–4588. doi:10.1021/am507443p
35. Sheng D, Deng L, Li P, et al. Perfluorocarbon nanodroplets with deep tumor penetration and controlled drug delivery for ultrasound/fluorescence imaging guided breast cancer therapy. *ACS Biomater Sci Eng.* 2021;7(2):605–616. doi:10.1021/acsbmaterials.0c01333



36. Pan R, Zhang H, Zhao X, et al. Preparation and anti-tumor activity study of folic acid modified crebanine polyethyleneglycol-poly(lactic acid hydroxyacetic acid) copolymer nanoparticles in vitro. *Chin Traditional Herbal Drugs*. 2023;54(20):6643–6656.
37. Tian Y, Liu Z, Zhang L, et al. Apatinib-loaded lipid nanobubbles combined with ultrasound-targeted nanobubble destruction for synergistic treatment of HepG2 cells in vitro. *Oncotargets Ther*. 2018;11:4785–4795. doi:10.2147/OTT.S170786
38. Liu H, Zhang R, Zhang D, et al. Cyclic RGD-decorated liposomal gossypol AT-101 targeting for enhanced antitumor effect. *Int J Nanomed*. 2022;17:227–244. doi:10.2147/IJN.S341824
39. Liu H, Marquez RT, Wu X, et al. A non-intrusive evaluation method for tumor-targeting characteristics of nanomedicines based on in vivo near-infrared fluorescence imaging. *J Mater Chem B*. 2019;7(31):4751–4757. doi:10.1039/C9TB00882A
40. Ma Y, Wu H, Zhang Z, Liu C, Yuan C. Acute toxicity and antiarrhythmia effect of crebanine. *Chinese J of Modern Applied Pharmacy*. 2005;5(2):18–19. doi:10.3724/j.issn.1000-0518.1988.2.1822
41. Song J, Ye H, Jiang S, et al. An acid response IR780-based targeted nanoparticle for intraoperative near-infrared fluorescence imaging of ovarian cancer. *Int J Nanomed*. 2022;17:4961–4974. doi:10.2147/IJN.S375145
42. Zhong C, Chen J, Ling Y, et al. Indocyanine green-loaded nanobubbles targeting carbonic anhydrase IX for multimodal imaging of renal cell carcinoma. *Int J Nanomed*. 2023;18:2757–2776. doi:10.2147/IJN.S408977
43. Wang J, Liao H, Ban J, et al. Multifunctional near-infrared dye IR-817 encapsulated in albumin nanoparticles for enhanced imaging and photothermal therapy in melanoma. *Int J Nanomed*. 2023;18:4949–4967. doi:10.2147/IJN.S425013
44. Zhang S, Sun J. Nano-drug delivery system for the treatment of acute myelogenous leukemia. *Zhejiang Da Xue Xue Bao Yi Xue Ban*. 2022;51(2):233–240. [English]. doi:10.3724/zdxbyxb-2022-0084
45. Guo X, Mei J, Jing Y, et al. Curcumin-loaded nanoparticles with low-intensity focused ultrasound-induced phase transformation as tumor-targeted and pH-sensitive theranostic nanopatform of ovarian cancer. *Nanoscale Res Lett*. 2020;15(1):73. doi:10.1186/s11671-020-03302-3
46. Somaglino L, Mousnier L, Giron A, et al. In vitro evaluation of polymeric nanoparticles with a fluorine core for drug delivery triggered by focused ultrasound. *Colloids Surf B Biointerfaces*. 2021;200:111561. doi:10.1016/j.colsurfb.2021.111561
47. Ma Y, Shang Q, Bai Y, et al. Study on pharmacokinetics of crebanine injection in rabbits. *China J of Chinese Materia Medica*. 2007;32(7):630–632.
48. Jiménez A, Rufo M, Paniagua JM, et al. Acoustic characterization study of beef loins using ultrasonic transducers. *Sensors*. 2023;23(23):9564. doi:10.3390/s23239564
49. Nowicki A. Safety of ultrasonic examinations; thermal and mechanical indices. *Med Ultrason*. 2020;22(2):203–210. doi:10.11152/mu-2372
50. Casciaro S, Demitri C, Conversano F, et al. Experimental investigation and theoretical modelling of the nonlinear acoustical behaviour of a liver tissue and comparison with a tissue mimicking hydrogel. *J Mater Sci Mater Med*. 2008;19(2):899–906. doi:10.1007/s10856-007-3007-8
51. Song KH, Harvey BK, Borden MA. State-of-The-art of microbubble-assisted blood-brain barrier disruption. *Theranostics*. 2018;8(16):4393–4408. doi:10.7150/thno.26869
52. Lin L, Dou C, Zhang K, et al. Study on the anti-cell proliferation activity of hydroxycamptothecin nanoparticles mediated by ultrasound. *Chinese Traditional Patent Med*. 2023;45(11):3753–3758.
53. Pan R, Tang J, Zhang H, et al. Effects of folic acid modified PEG-PLGA crebanine nanoparticles combined with ultrasonic irradiation on subcutaneous tumor growth of liver cancer in mouse. *Chin J Exp Traditional Med Formulae*. 2023;54(20):6643–6656.1–12.

International Journal of Nanomedicine

Dovepress

## Publish your work in this journal

The International Journal of Nanomedicine is an international, peer-reviewed journal focusing on the application of nanotechnology in diagnostics, therapeutics, and drug delivery systems throughout the biomedical field. This journal is indexed on PubMed Central, MedLine, CAS, SciSearch®, Current Contents®/Clinical Medicine, Journal Citation Reports/Science Edition, EMBase, Scopus and the Elsevier Bibliographic databases. The manuscript management system is completely online and includes a very quick and fair peer-review system, which is all easy to use. Visit <http://www.dovepress.com/testimonials.php> to read real quotes from published authors.

Submit your manuscript here: <https://www.dovepress.com/international-journal-of-nanomedicine-journal>